Mineralogical Magazine, December 2017, Vol. 81(6), pp. 1551–1576

Trace-element compositions of sapphire and ruby from the eastern Australian gemstone belt

JACQUELINE WONG[1,*], CHARLES VERDEL[1] AND CHARLOTTE M. ALLEN[2,3]

[1] School of Earth and Environmental Sciences, University of Queensland, St Lucia, QLD 4072, Australia
[2] Institute for Future Environments, Queensland University of Technology, Brisbane, QLD 4001, Australia
[3] School of Earth, Environmental and Biological Sciences, Queensland University of Technology, Brisbane, QLD 4001, Australia

[*Received 12 October 2016; Accepted 14 February 2017; Associate Editor: Stuart Mills*]

ABSTRACT

Significant uncertainty surrounds the processes involved in the formation of basalt-hosted corundum, particularly the role that the mantle plays in corundum generation. Some previous studies have suggested that trace-element ratios (namely, Cr/Ga and Ga/Mg) are useful for distinguishing two types of corundum: 'magmatic' and 'metamorphic', designations that include mantle and crustal processes. However, recent studies, including this one, have discovered transitional groups between these end-members that are difficult to classify. We used laser ablation inductively coupled plasma mass spectrometry (LA–ICP–MS) to measure trace-element concentrations in sapphire and ruby crystals from eight alluvial deposits that span a significant length of the eastern Australian gemstone belt. Additionally, we collected LA–ICP–MS U–Pb and trace-element data from zircon megacrysts at Weldborough, Tasmania, which is also within the gemstone belt. Our sapphire and ruby results reveal a continuum in trace-element compositions, an observation that raises questions regarding previous classifications that ascribe corundum from basalt-hosted gemfields to either 'magmatic' or 'metamorphic' sources. The spatial association of basalt-related gemfields in eastern Australia with a long-lived convergent margin suggests a link between corundum formation and Al-enrichment of the mantle wedge during periods of subduction.

KEYWORDS: trace-element geochemistry, LA–ICP–MS, corundum, sapphire, ruby, eastern Australian gemstone belt, subduction zone, zircon.

Introduction

SAPPHIRES and rubies are gem varieties of corundum (Al_2O_3) that have very 'pure' compositions: they generally contain <1 wt.% of other elements because few elements can easily substitute for Al in the corundum structure. Nevertheless, minor and trace amounts of chromophores (colour-causing elements) give rise to the distinctive hues of these gemstones (MacNevin, 1972; Nassau, 2001). Sapphires and rubies are commonly found in alluvial deposits that are typically associated spatially with Cenozoic alkali basalts and accompanying gem-quality zircon (e.g. Graham *et al*., 2008; Giuliani *et al*., 2014). Basalt-related gemfields of this type in southeastern Asia, China, Russia and eastern Australia have been collectively referred to as 'west Pacific continental margin' deposits (Graham *et al*., 2008), a designation that highlights their tectonic association with current or ancient convergent margins (Fig. 1). Other examples of basalt-related gemfields occur in Madagascar, Nigeria, Cameroon and the French Massif Central (Giuliani *et al*., 2014).

Eastern Australia has the broadest spatial distribution of basalt-related alluvial gemfields in the world (Fig. 2). In the case of Australian basalt-related corundum, the conditions required for formation are enigmatic: corundum crystals have mineralogical associations suggesting a wide range

*E-mail: jacqueline.wong@uqconnect.edu.au
https://doi.org/10.1180/minmag.2017.081.012

© *2017 The Mineralogical Society*

https://doi.org/10.1180/minmag.2017.081.012 Published online by Cambridge University Press

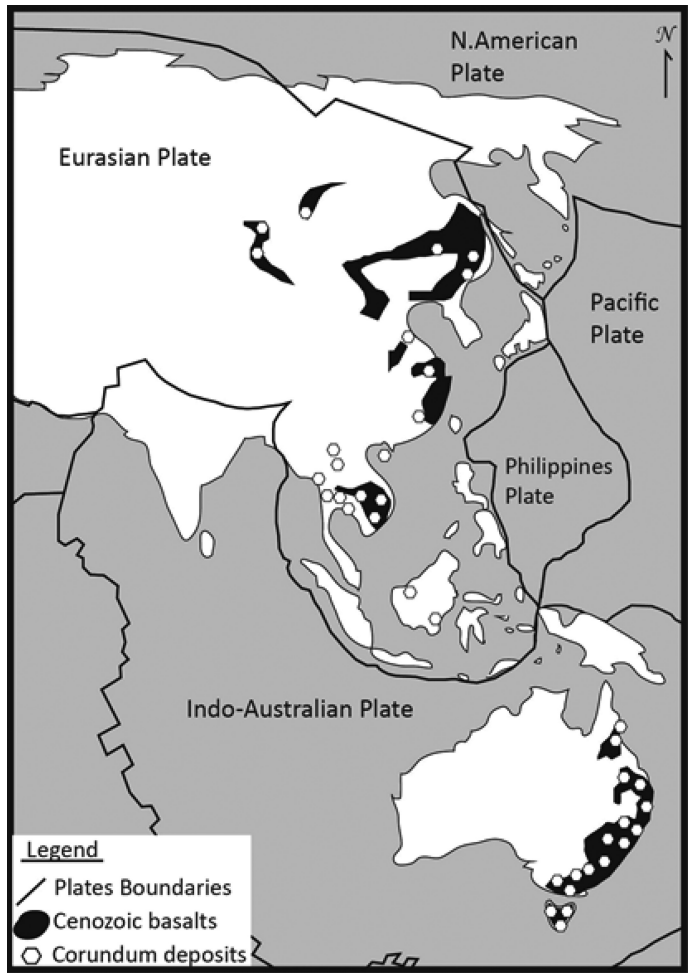


FIG. 1. Map of the western Pacific continental margin showing spatial association between intraplate Cenozoic basalts (black areas) and gem corundum deposits (unfilled hexagons). Taken and adapted from Graham *et al*. (2008).

of pressure, temperature and geochemical conditions during their generation (e.g. Sutherland and Coenraads, 1996; Sutherland *et al*., 2003; Zaw *et al*., 2006). In eastern Australia, sapphires and rubies seem to have been transported to the surface as xenocrysts in alkali basalts (see Table 1), but they are also found in xenoliths in rare instances (Sutherland *et al*., 2003, 2015). Our current understanding is that the corundum xenocrysts were originally formed in the lower crust or mantle, where unusual bulk-rock compositions and pressure–temperature conditions facilitated corundum crystallization (e.g. Lishmund and Oakes, 1989; Coenraads *et al*., 1990; Robertson and Sutherland, 1992; Coenraads, 1994; Levinson and Cook, 1994). Several models for sapphire formation have been proposed for eastern Australian corundum, including crystallization near the Moho (e.g. Robertson and Sutherland, 1992), metamorphism of subducted Al-rich material (e.g. Levinson and Cook, 1994), and melting of amphibole-bearing lithospheric mantle (Sutherland *et al*., 1998*a*). Models for the formation of basalt-related corundum on other continents include low-degree partial melting of an upper mantle source (Khamloet *et al*., 2014; Giuliani *et al*., 2015), partial melting of crustal anorthosites in a subduction zone setting (Palke *et al*., 2016), as well as 'hybrid' models

https://doi.org/10.1180/minmag.2017.081.012 Published online by Cambridge University Press

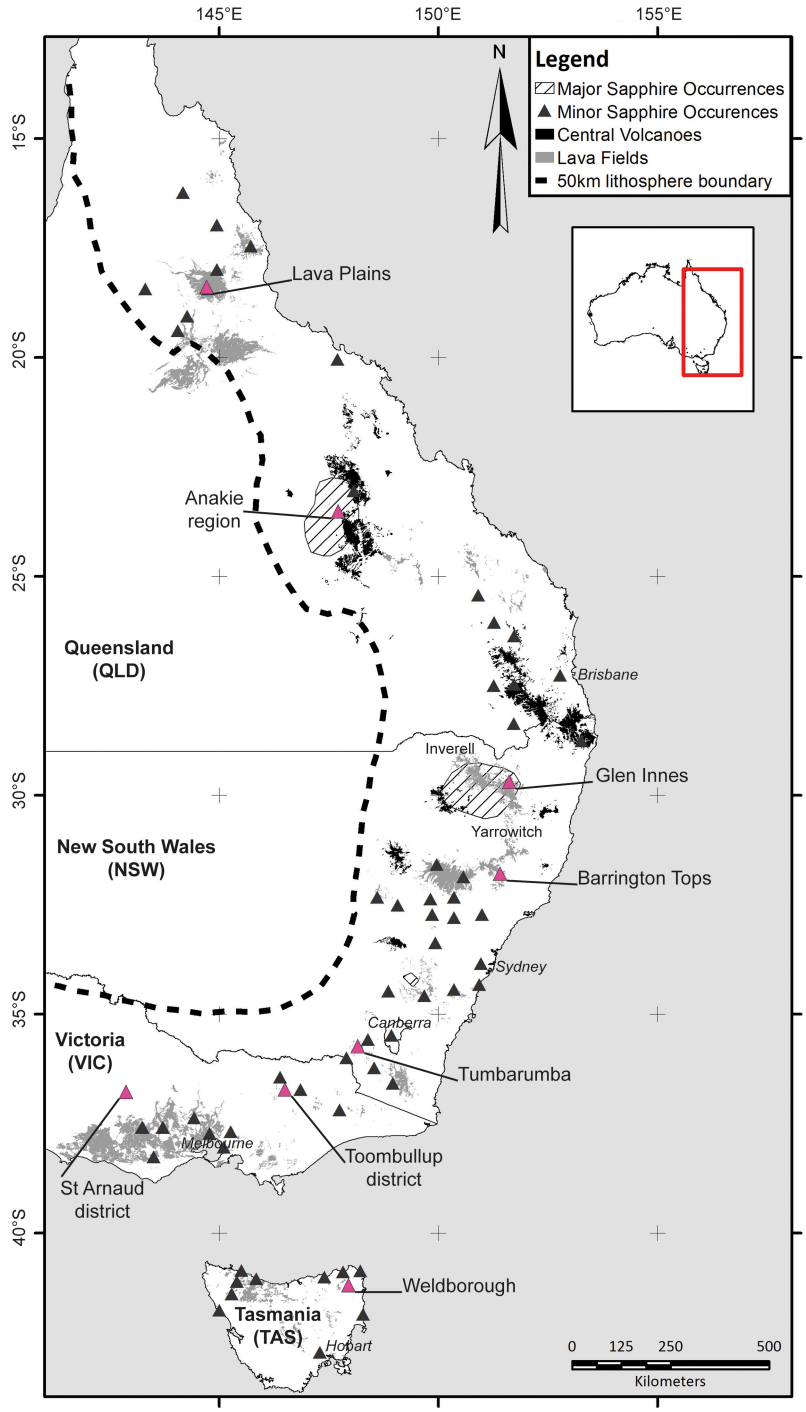


FIG. 2. Map of the eastern Australian gemstone belt showing major and minor sapphire occurrences associated with Cenozoic alkali basalts (central volcanoes and lava-fields) along the thinner (~50 km thick) eastern Australian lithosphere (Fishwick *et al*., 2008). Geological units for volcanic provinces from Raymond *et al*. (2012). Gem deposits compiled from Sutherland and Abduriyim (2009). Pink triangles highlight the deposits studied.

https://doi.org/10.1180/minmag.2017.081.012 Published online by Cambridge University Press

TABLE 1. Gem fields and associated lava-fields of eastern Australia, showing associated lava-field eruption age(s) or alternate source in italics.

Gemfield	Associated lava-field	Age of lava-field (Ma)
Lava Plains	McBride	3–0.02[1]
Anakie region	Hoy Province	66.8–17.3[2]
Glen Innes	Central	39.4–30.5, 26.2–19.8[4]
Barrington Tops	Barrington Province	59.4–41[5]
Tumbarumba	Snowy Mountains Province	23.7–18[3,6]
Toombullup District	Older Volcanics, Group 3	45.9–31[3,7]
St. Arnaud District	Older Volcanics, Groups 1 & 2	95–38[3]
	Sapphires from St. Arnaud distract are suggested to be sourced from White Hills Gravel[8]	*Maximum age of 74.5 Ma*[8]
Weldborough	Weldborough Basalt	47.4–46.2[9]

[1]Zhang *et al*. (2001); [2]Cohen (2007); [3]Johnson *et al*. (1989); [4]Sutherland *et al*. (1993); [5]Sutherland and Fanning (2001); [6]Sutherland *et al*. (2002); [7]Henley and Webb (1990); [8]Birch *et al*. (2007); [9]Sutherland and Wellman (1986).

involving multiple sources (Guo *et al*., 1996; Upton, 1999; Yui *et al*., 2003; Giuliani *et al*., 2007). This study explores regional patterns in trace-element compositions of eastern Australian corundum in order to constrain further the petrogenesis of basalt-hosted gem corundums.

Background and classification of gem corundum

The colour variation in sapphires and rubies arises from differences in the concentrations of the chromophore elements $Fe^{2+/3+}$, Cr^{3+}, Ti^{4+} and V^{3+}. Sapphires and rubies are distinguished on the basis of colour and Cr concentrations: rubies are red; and sapphires are any other colour. Intervalence charge transfer between adjacent Fe^{2+} and Ti^{4+} results in the blue colour of sapphires (Pisutha-Arnond *et al*., 2006); metal charge transfers between O^{2-} and Fe^{2+}/Fe^{3+} creates yellow to green sapphires (Fritsch and Rossman, 1988); Cr^{3+} enrichment is responsible for the red colour of rubies (Fritsch and Rossman, 1987); and slate to purple colours can be caused by substitution of V^{3+} (Zaw *et al*., 2015), as well as Cr, Fe and Ti. Chromium concentration, in particular, seems to largely govern the colour of corundum.

Sapphire and ruby deposits are typically divided into two overall groups: primary deposits and secondary deposits. Primary deposits are those with gems found within the rocks in which they crystallized (Simonet *et al*., 2008). In contrast, secondary deposits include xenocrystical gems that were transported to the surface by volcanism, as well as gems eroded from their host rocks and re-deposited in alluvial deposits (Simonet *et al*., 2008). Primary corundum can be further subdivided into igneous or metamorphic types, for example 'igneous' for corundum in syenites or monzonite dykes (Simonet *et al*., 2004), and 'metamorphic' for corundum in amphibolite, marble, metasomatite, pegmatite and gneiss (Pham *et al*., 2004; Giuliani *et al*., 2005; Stern *et al*., 2013). Some basalt-derived corundum crystals occur both in xenoliths and as xenocrysts, and they can be either magmatic or metamorphic (Sutherland *et al*., 2003, 2015; Giuliani *et al*., 2009; Chualaowanich *et al*., 2014; Rakotosamizanany *et al*., 2014).

The ultimate source rock composition and crystallization conditions for corundum are clearly more difficult to ascertain for secondary corundum deposits (Sutherland, 1996; Pham *et al*., 2004; Graham *et al*., 2008; Giuliani *et al*., 2014), which are the focus of this study. However, previous studies have suggested that secondary corundum of the 'magmatic' and 'metamorphic' types have differences in colour and size: magmatic corundum generally consists of large (>12 mm) and transparent to opaque crystals that are typically blue, yellow and green in colour, whereas metamorphic corundum is smaller (2–5 mm) and paler in colour, including blue, pink and purple sapphires of less clarity, in addition to ruby (e.g. Sutherland *et al*., 1998*b*). Given the link between colour and trace-element composition described above, these differences suggest an underlying variability in the trace-element compositions of the two groups.

https://doi.org/10.1180/minmag.2017.081.012 Published online by Cambridge University Press

https://doi.org/10.1180/minmag.2017.081.012 Published online by Cambridge University Press

TABLE 2. Calculated fractionation factors (α) between basalt, olivine, anorthoclase in relation to corundum, using equations from Criss (1999) and Sharp (2007).

	Basalt ($\delta^{18}O$)			Corundum ($\delta^{18}O$)			Fractionation factors				
	Min	Max	Mean	Min	Max	Mean	Min	Max	Mean		
Tunkin depression, Russia[1]	6.1			9.1			0.997			$\alpha_{Basalt\text{-}Corundum}$	
Dak Nong, Vietnam[2]	5.7			6	6.9	6.5	0.9997	0.9988	0.999	Minimum	0.997
	5	5.2	5.1				0.9981	0.999	0.999	Maximum	0.9997
	Olivine ($\delta^{18}O$)			Corundum ($\delta^{18}O$)			Fractionation factors				
	Min	Max	Mean	Min	Max	Mean	Min	Max	Mean		
Podgelbanochnyi volcano, Russia[1]	5			5.5	6.4	5.95	0.9986	0.9995	0.999		
Denchai alluvial deposit, Thailand[3]	4.9	5.1	5.05	4.7	6.1	5.45	0.9988	1.0004	1	$\alpha_{Olivine\text{-}Corundum}$	
Chanthaburi-Trat alluvial sapphires, Thailand[4]	4.8	5	4.888	5.1	6.2	5.86	0.9986	0.9999	0.999	Minimum	0.9986
Tok Phrom alluvial rubies[4]				2.4	3.9	3.007	1.0009	1.0026	1.002	Maximum	1.0037
Bo Na Wong alluvial rubies[4]				2.3	3.1	2.493	1.0017	1.0027	1.002		
Nong Bon alluvial rubies[4]				1.6	4.2	2.853	1.0006	1.0034	1.002		
Bo Rai alluvial rubies[4]				1.3	3.7	2.48	1.0011	1.0037	1.002		
	Anorthoclase ($\delta^{18}O$)			Corundum ($\delta^{18}O$)			Fractionation factors				
Anorthoclase xenolith, Menet trachyte[5]	7.7	7.9		4.4			1.0033	1.0079		$\alpha_{Feldspar\text{-}Corundum}$	
										Minimum	1.0033
										Maximum	1.0079

Data were retrieved from existing studies, referenced in foot note.
[1]Vysotsky *et al.* (2009); [2]Garnier *et al.* (2005); [3]Yui *et al.* (2003); [4]Yui *et al.* (2006); [5]Giuliani *et al.* (2009).

As such, trace-element compositions (as well as mineral inclusions and O-isotope ratios, discussed below) have been utilized previously in an effort to constrain their original sources of alluvial corundum and assist in the magmatic *vs*. metamorphic designation and discrimination. Distinctions in Cr_2O_3/Ga_2O_3 ratios, as measured with electron microprobe and LA–ICP–MS, were readily apparent in alluvial corundum from eastern Australia and SE Asia and seemed to justify the use of this ratio to delineate different sources of corundum (Sutherland *et al*., 1998*b*; Saminpanya *et al*., 2003; Abduriyim and Kitawaki, 2006). Cr_2O_3/Ga_2O_3 <1 denoted magmatic corundum, while Cr_2O_3/Ga_2O_3 >3 indicated metamorphic corundum. Ga/Mg has been proposed as another useful ratio for distinguishing the source of blue sapphires (Peucat *et al*., 2007).

Mineral inclusions are another source of information on the petrogenesis of corundum. Some of these inclusions (rutile and Fe–Ti oxides) can result in the asterism observed in corundum (Moon and Phillips, 1984). Other common mineral inclusions within magmatic sapphires include Nb-Ta oxides, alkali feldspars, low-Ca plagioclase and zircon (Guo *et al*., 1996). Rare inclusions include sulfides, spinel and Th-, Ce-rich phosphates. These inclusions suggest mixing between a silicic component and a carbonatitic/Si-poor component at crustal levels or crystallization from felsic magmas (Guo *et al*., 1996; Sutherland *et al*., 1998*a*). Sapphires in Thailand and Vietnam contain high-K and high-Na silicate melt inclusions and CO_2-rich fluid inclusions, which suggest a magmatic source (Limtrakun *et al*., 2001; Izokh *et al*., 2010). In contrast, the association of sapphirine, Al-rich diopside, spinel and garnet with high-Cr/Ga corundum in some SE Asian and eastern Australian alluvial deposits has been cited to suggest a metamorphic origin for these corundum occurrences (Sutherland and Coenraads, 1996; Sutherland *et al*., 1998*a*; Saminpanya and Sutherland, 2011).

Oxygen–isotope ratios ($\delta^{18}O$) are yet another source indicator for corundum. Alluvial sapphires from basaltic provinces (basalt–syenite–mafic rock) have a wide range of $\delta^{18}O$ from 3.0 to 8.2‰ (Giuliani *et al*., 2009). Alluvial rubies have lower $\delta^{18}O$, as low as 1.2–1.3‰ (Yui *et al*., 2006; Rakotosamizanany *et al*., 2014). Low $\delta^{18}O$ in alluvial rubies probably reflects the involvement of crustal fluids during metamorphism of mafic to ultramafic protoliths, which might have been mantle to oceanic crustal material. The range for alluvial sapphires overlaps with the $\delta^{18}O$ of mantle-derived rocks (~5–6‰), but includes higher values (6–8‰) that might indicate contributions from a metasedimentary component. In contrast, corundum crystals from skarns and marbles have crustal $\delta^{18}O$ (7.8–24‰). Fractionation factors between basalt and corundum have not been fully

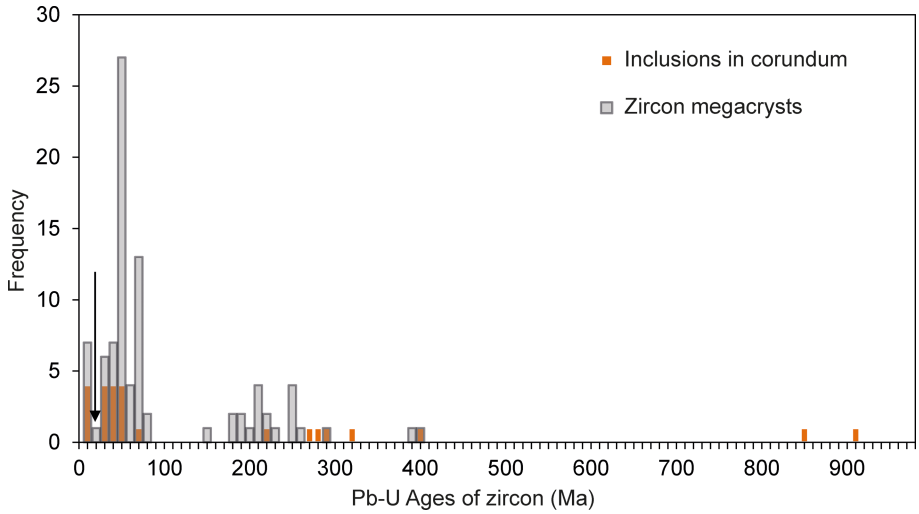


FIG. 3. Compilation of U–Pb ages from zircon megacrysts and zircon inclusions in eastern Australian corundum, as determined with SHRIMP and LA–ICP–MS (Coenraads *et al*., 1990; Sutherland and Fanning, 2001; Sutherland *et al*., 2002, 2016; Birch *et al*., 2006; Zaw *et al*., 2006; Abduriyim *et al*., 2012). An arrow indicates the age of the zircons associated with corundum from Weldborough (this study).

https://doi.org/10.1180/minmag.2017.081.012 Published online by Cambridge University Press

TABLE 3. Trace-element concentrations (Mg, Ti, V, Cr, Fe and Ga) of corundum from LA–ICP–MS, reported as mean per individual sample in ppm.

		Mg	Ti	V	Cr	Fe	Ga
Lava Plains, northern Queensland							
D57524-010 ($n = 4$)	Mean	9.2	88.2	11.5	1.2	3551.0	128.0
Light blue	1 std	3.5	53.1	0.7	0.3	271.5	4.7
	%RSD	37.8	60.2	5.9	21.9	7.6	3.6
D57524-0006 ($n = 4$)	Mean	37.5	1394.5	14.0	0.9	7256.9	253.8
Blue	1 std	5.2	245.3	1.0	0.1	411.6	10.4
	%RSD	14.0	17.6	7.1	16.1	5.7	4.1
D57524-004 ($n = 4$)	Mean	13.0	121.7	7.7	1.3	4647.7	130.6
Blue	1 std	1.7	60.4	1.6	0.0	39.5	24.2
	%RSD	13.0	49.6	20.7	3.2	0.8	18.5
Anakie Region, central Queensland							
D816-003 ($n = 3$)	Mean	8.7	437.4	19.9	0.2	5216.9	365.4
Dark Blue	1 std	3.4	253.6	2.0	0.0	393.5	22.2
	%RSD	38.9	58.0	10.2	0.0	7.5	6.1
D816-027 ($n = 4$)	Mean	32.5	41.4	5.2	0.2	8410.9	197.5
Yellow	1 std	6.2	3.5	0.2	0.0	1324.9	11.8
	%RSD	19.2	8.5	3.4	20.2	15.8	6.0
D816-029 ($n = 2$)	Mean	7.5	16.5	4.0	1.2	6007.4	153.6
Green-yellow	1 std	8.5	14.1	1.1	1.6	1482.9	21.7
	%RSD	113.5	85.2	28.5	124.4	24.7	14.1
D44054-004 ($n = 2$)	Mean	8.3	84.3	8.8	0.2	5563.0	152.0
Blue-colourless	1 std	0.2	4.2	0.5	0.1	379.1	22.1
	%RSD	2.3	4.9	5.4	47.1	6.8	14.5
D44054-008 ($n = 2$)	Mean	24.8	40.8	8.0	19.9	8780.8	123.8
Green-yellow	1 std	1.0	0.6	0.0	0.2	374.2	5.5
	%RSD	4.2	1.4	0.3	1.2	4.3	4.4
D44054-009 ($n = 2$)	Mean	14.2	103.5	7.0	17.5	3373.7	124.2
Blue	1 std	3.5	18.8	0.3	3.3	118.5	0.2
	%RSD	25.0	18.1	4.3	18.9	3.5	0.2
D48171-002 ($n = 2$)	Mean	8.6	340.4	7.6	7.0	4635.4	129.1
Blue	1 std	6.5	429.2	3.2	7.6	221.7	8.2
	%RSD	75.8	126.1	41.9	109.3	4.8	6.4
D48171-003 ($n = 3$)	Mean	6.0	77.8	7.8	0.7	4753.0	131.6
Blue	1 std	2.1	6.5	0.3	0.8	254.8	1.1
	%RSD	35.5	8.3	3.2	115.6	5.4	0.8
Glen Innes, New South Wales							
GI-003 ($n = 2$)	Mean	1.9	38.0	4.2	1.0	2064.4	101.7
Light blue	1 std	0.3	1.0	0.2	0.8	13.2	1.9
	%RSD	14.5	2.6	3.6	83.9	0.6	1.9
Barrington Top, New South Wales							
D43427-004 ($n = 2$)	Mean	43.6	69.7	14.8	40.4	8236.9	90.6
Light blue	1 std	2.4	3.6	3.7	51.8	2349.2	42.4
	%RSD	5.4	5.2	25.0	128.2	28.5	46.8
D43427-005 ($n = 2$)	Mean	49.4	66.6	51.2	71.1	5234.2	26.8
Light blue	1 std	0.8	6.4	1.0	3.2	40.2	3.7
	%RSD	1.7	9.7	1.9	4.5	0.8	13.8
D43427-009 ($n = 2$)	Mean	323.5	86.8	12.0	88.9	5390.0	75.2
Pink	1 std	411.4	103.1	5.2	118.4	3035.2	82.1
	%RSD	127.2	118.8	43.1	133.2	56.3	109.2

(continued)

https://doi.org/10.1180/minmag.2017.081.012 Published online by Cambridge University Press

TABLE 3. (*contd*.)

		Mg	Ti	V	Cr	Fe	Ga
Tumbarumba, New South Wales							
D53381-001 ($n = 2$)	Mean	33.1	469.9	9.6	0.2	8393.7	189.4
Dark blue	1 std	30.5	240.5	3.4	0.0	2196.7	79.8
	%RSD	92.3	51.2	35.7	20.2	26.2	42.1
D53381b-007 ($n = 4$)	Mean	30.1	525.5	15.8	117.2	7185.9	142.7
Blue	1 std	6.9	157.9	0.6	51.0	629.3	11.8
	%RSD	22.9	30.0	3.8	43.6	8.8	8.3
D53381b-010 ($n = 2$)	Mean	6.5	90.3	5.1	2.4	6237.7	130.0
Yellow-blue	1 std	7.0	116.3	2.5	1.4	1836.4	5.3
	%RSD	107.7	128.8	49.3	57.4	29.4	4.1
Carapooee, St Arnaud district, western Victoria							
M46183 ($n = 2$)	Mean	101.5	150.4	44.1	2546.5	2585.7	30.4
Dark pink	1 std	10.4	17.3	3.0	39.5	286.2	0.8
	%RSD	10.2	11.5	6.7	1.6	11.1	2.5
M48692-001 ($n = 4$)	Mean	186.0	299.6	62.6	3092.9	5816.3	145.6
Dark red	1 std	40.2	51.0	12.1	1040.2	580.5	83.4
	%RSD	21.6	17.0	19.3	33.6	10.0	57.3
M48692-002 ($n = 2$)	Mean	232.1	233.7	22.6	263.0	7247.1	23.9
Dark blue	1 std	6.2	31.1	3.3	32.4	117.8	2.2
	%RSD	2.7	13.3	14.5	12.3	1.6	9.4
M48692-010 ($n = 4$)	Mean	132.3	266.8	48.6	19.0	6453.3	37.6
Blue	1 std	4.6	81.5	6.5	5.0	439.2	2.2
	%RSD	3.5	30.6	13.4	26.1	6.8	5.7
M48692-016 ($n = 4$)	Mean	43.8	43.7	7.2	34.7	6960.5	68.0
Pale green	1 std	0.8	1.5	0.3	12.0	594.6	4.4
	%RSD	1.8	3.5	4.7	34.4	8.5	6.5
M48692-017 ($n = 4$)	Mean	46.9	57.7	11.6	76.4	9013.6	62.6
Brown-yellow	1 std	16.3	8.2	0.8	4.8	829.3	3.4
	%RSD	34.8	14.1	7.1	6.3	9.2	5.4
M48692-020 ($n = 4$)	Mean	107.7	90.3	33.6	383.5	3596.6	48.3
Light purple-pink	1 std	1.9	4.1	1.6	72.1	278.9	3.3
	%RSD	1.7	4.6	4.6	18.8	7.8	6.8
Toombullup district, eastern Victoria							
M50863-001 ($n = 2$)	Mean	18.6	225.4	34.6	17.7	2169.7	301.6
Grey-blue	1 std	0.6	55.4	0.6	2.1	105.3	1.9
	%RSD	3.0	24.6	1.8	11.6	4.9	0.6
M50863-002 ($n = 4$)	Mean	15.3	159.3	23.3	3.5	3481.9	182.5
Light grey	1 std	3.4	141.7	4.0	0.7	415.3	18.9
	%RSD	22.0	88.9	17.1	20.6	11.9	10.3
M50863-003 ($n = 4$)	Mean	41.5	89.8	6.6	1.0	13,649.0	435.5
Grey-blue	1 std	8.4	32.9	0.8	0.6	819.8	29.3
	%RSD	20.2	36.7	12.2	56.1	6.0	6.7
M44392-003 ($n = 4$)	Mean	26.3	59.2	2.9	1.2	13293.7	117.4
Colourless	1 std	1.7	15.3	0.2	0.3	515.9	12.2
	%RSD	6.5	25.9	7.5	24.2	3.9	10.4
Weldborough, Tasmania							
LR-001 ($n = 4$)	Mean	23.0	5.2	8.8	1.5	3273.7	229.0
Colourless	1 std	1.4	2.0	0.6	0.4	53.8	4.2
	%RSD	5.9	38.7	7.3	28.9	1.6	1.8
LR-002 ($n = 4$)	Mean	3.7	60.6	0.9	1.0	3751.4	180.9
Light blue	1 std	2.8	43.2	0.1	0.4	131.4	17.1
	%RSD	75.2	71.2	7.9	43.7	3.5	9.5

(continued)

https://doi.org/10.1180/minmag.2017.081.012 Published online by Cambridge University Press

TABLE 3. (*contd*.)

		Mg	Ti	V	Cr	Fe	Ga
LR-003 ($n = 4$)	Mean	11.4	7.7	2.6	1.9	3704.4	170.1
Light blue	1 std	0.9	1.3	0.1	0.2	221.7	1.4
	%RSD	7.6	16.4	4.5	8.9	6.0	0.8
LR-004 ($n = 4$)	Mean	7.9	417.7	22.2	32.0	4615.8	189.6
Blue	1 std	1.3	120.2	4.0	30.4	193.5	12.3
	%RSD	16.5	28.8	18.1	95.3	4.2	6.5

Data reduction by *Iolite* software (Paton *et al*., 2011), and recalculated based on an assumption of 98 wt.% Al_2O_3. Sample names are given in the first column for individual crystals; *n* represents number of spot analyses. 1 standard deviation errors (1 std) and relative standard deviation percentages (RSD%) have been calculated for each individual sample.

established, but here we estimate the fractionation factor (α) between basalt–corundum, olivine–corundum and anorthoclase–corundum using compiled data and the following equations from Criss (1999) and Sharp (2007):

$$\Delta_{A-B} = \delta_A - \delta_B \quad \text{and} \quad \Delta_{A-B} \approx 1000(\alpha_{A-B} - 1)$$

where A and B refer to two different phases in the same rock. On the basis of our data compilation, $\alpha_{basalt-corundum}$ ranges from 0.9970 to 0.9997, $\alpha_{olivine-corundum}$ ranges from 0.9958 to 1.0004, and $\alpha_{anorthoclase-corundum}$ ranges from 1.0033 to 1.0079 (See Table 2). Overall, our estimates suggest relatively minor O fractionation between corundum and basalt, olivine and anorthoclase.

Finally, in addition to the two-fold, 'magmatic' and 'metamorphic' designations described above, trace-element concentrations and colour absorption spectra (EDXRF) investigations of Al_2O_3 from both the Tumbarumba and Cudgegong-Macquarie River areas of eastern Australia concluded that some corundum has a 'metasomatic' origin because they have features intermediate to the proposed magmatic and metamorphic suites (Sutherland *et al*., 2002, 2003). Corundum from Tumbarumba with transitional trace-element ratios between 'metamorphic' and 'igneous' was proposed to be metasomatic in origin and possibly related to interactions with Cr-bearing serpentinites (Sutherland *et al*., 2002). Other deeper mantle origins have been proposed for gems in the Macquarie River area of New South Wales because of high temperature and pressure estimates (1200°C and 2.5 GPa; Sutherland *et al*., 2003), suggesting that a mantle origin of ruby is possible, even though rubies are widely regarded as metamorphic minerals.

Geological background

The eastern Australian gemstone belt

The eastern Australian gemstone belt (Fig. 2) is a chain of alluvial sapphire, ruby and zircon deposits that extends along the eastern Australian margin from Cooktown, Queensland, in the north, to Tasmania in the south (Lishmund and Oakes, 1989; Giuliani *et al*., 2014). Major corundum deposits include Anakie (Queensland) and the Inverell–Glen Innes area (New South Wales, NSW), as well as minor sapphire occurrences farther south in NSW, Victoria and Tasmania. Barrington Tops, Yarrowitch, Cudgegong–Macquarie Rivers and Tumbarumba in NSW, as well as the St Arnaud district in Victoria, are examples of Australian ruby-bearing deposits (Sutherland and Coenraads, 1996; Sutherland *et al*., 2002, 2009; Birch, 2008). The Victorian gemfields have not been studied extensively, but Birch and Henry (1997) and Birch (2008) provide detailed descriptions of these gemfields.

The two main suites of gem corundum within the eastern Australian gemstone belt are a blue–green–yellow (BGY) 'magmatic' suite of sapphires, and a partly pale-coloured 'metamorphic' suite that contains sapphire and minor ruby (Sutherland *et al*., 1998*b*). Geochemical data (Ga and Mg concentrations and $\delta^{18}O$) have been utilized to distinguish magmatic and metamorphic sources, and, using the conventions described above, BGY 'magmatic' sapphires are predominant in eastern Australia (e.g. Sutherland *et al*., 2009). Gemfields that contain ruby have been characterized as having multiple or bimodal sources (Sutherland *et al*., 2002, 2003). Rare occurrences of sapphires in xenoliths have been described from Mt Leura near Lava Plains (Stephenson, 1976; Sutherland *et al*., 2015), and the

https://doi.org/10.1180/minmag.2017.081.012 Published online by Cambridge University Press

sapphires in xenoliths from Lava Plains are proposed to be metasomatic (Sutherland *et al*., 2015).

Eastern Australian Cenozoic basaltic volcanism

Corundum in the eastern Australian gemstone belt seems to have been transported to the surface by Cenozoic intraplate basaltic magmas, the locations of which are related to, and perhaps controlled by, a region of particularly thin lithosphere in easternmost Australia (Fig. 2; Fishwick *et al*., 2008; Davies *et al*., 2015). Intraplate volcanism along the eastern Australian continental margin is complex and occurred from late Mesozoic time to relatively recently (<20 ka; Stephenson *et al*., 1998). There are two major volcanic province types in eastern Australia: 'central volcanoes', which may be related to hotspots, and 'lava-fields', which erupted in general association with rifting and episodic spreading phases of the Tasman Sea (90–64 Ma), Coral Sea (62–56 Ma), and Southern Ocean (O'Reilly and Zhang, 1995; Gaina *et al*., 1998; Vasconcelos *et al*., 2008; Sutherland *et al*., 2012, 2014; Price *et al*., 2014). An alternative model for generation of younger Cenozoic volcanism is by edge-driven convection, which has been proposed for the Newer Volcanic province in western Victoria (Davies and Rawlinson, 2014). Zircon megacrysts and zircon inclusions in corundum, commonly have mid-Cenozoic U–Pb ages that, in general, overlap with the dominant eruption ages of central volcanoes and lava-fields (Fig. 3; Coenraads *et al*., 1990; Sutherland and Fanning, 2001; Sutherland *et al*., 2002; Zaw *et al*., 2006; Birch *et al*., 2007; Abduriyim *et al*., 2012). However, zircon megacrysts and inclusions from Tumbarumba, NSW (Sutherland *et al*., 2002) and Weldborough, TAS (Zaw *et al*., 2006) have much older (Triassic and Ordovician/Silurian) U–Pb ages, indicating some degree of inheritance. Trace-element compositions of zircon megacrysts suggest a range of sources from ultramafic to felsic compositions, as well as thermal annealing during later basalt transport (Sutherland *et al*., 2016).

Eastern Australian sapphire and ruby deposits are associated most closely with lava-field provinces, which include both silica-undersaturated and -saturated rocks of alkali basaltic and tholeiitic compositions (Wellman and McDougall, 1974; Sutherland, 1978, 1996; Ewart *et al*., 1988; O'Reilly and Zhang, 1995). Incompatible trace-element concentrations, and Sr and Nd isotopic ratios (O'Reilly and Zhang, 1995), point towards a dominant oceanic island basalt source for most lava-fields from Queensland and NSW. Importantly, radiogenic isotope data suggest that the incorporation of sediments during former subduction-related processes and a metasomatized mantle probably played a role in the generation of lava-fields from northern Queensland and NSW (O'Reilly and Zhang, 1995). These same processes may have also been key in corundum formation, as discussed below.

Sampling and analytical procedure

A suite of eastern Australian sapphires and rubies was acquired from museum and academic donations, as well as by fossicking. Deposits studied include Lava Plains and the Anakie region in northern and central QLD; Glen Innes, Barrington Tops and Tumbarumba covering northern, central and southern NSW; Toombullup and St Arnaud districts covering eastern and western VIC; and Weldborough, representing the most well-known gemfield in Tasmania (Fig. 2). The selected sites thus span the entire eastern margin of Australia.

Samples from the Lava Plains, Glen Innes and Tumbarumba deposits consist of small (<5 mm) blue sapphires that vary from rounded to subangular. These crystals are rarely corroded. The Toombullup district gems are similar, but they also include colour-zoned green-grey crystals. The Anakie region corundum include both small and large (>12 mm) BGY crystals that generally have a hexagonal barrel shape, with some corroded crystals that have iron oxide/hydroxide staining. Barrington Tops and the St Arnaud district gems are the only two deposits in this study that contain rubies. Tumbarumba and the Cudgegong–Macquarie Rivers deposits have rare rubies, but they were not sampled in this study. The Barrington Tops samples analysed for this study only include small pale blue and pink crystals, whereas the St Arnaud district deposit includes the largest colour range (blue, green, yellow, pink, red, purple, brown), from crystals that are relatively small (<2 mm). Samples from Weldborough are well-rounded, typically small (2–5 mm), and pale blue and yellow. They are associated with zircon megacrysts (1–5 mm), some of which we dated (as described below).

Sample preparation and analytical procedure

Sapphires and rubies representing the widest variety of colour from the authors' collection of samples were selected for trace-element analysis, though this may not be a full representation of

https://doi.org/10.1180/minmag.2017.081.012 Published online by Cambridge University Press

https://doi.org/10.1180/minmag.2017.081.012 Published online by Cambridge University Press

TABLE 4. Geochronological data of Weldborough zircon megacrysts ($n = 39$)*.

				Isotopic ratios						Ages (Ma)			
Sample	Best age[1]	unc 2SE PROP[2]	Common Pb Corrected	$^{207}Pb/^{206}Pb$	2SE	$^{207}Pb/^{235}U$	2SE	$^{206}Pb/^{238}U$	2SE	$^{207}Pb/^{235}U$	2SE	$^{206}Pb/^{238}U$	2SE
1	14	3	Yes	0.11	0.23	0.038	0.021	0.0022	4E-04	38	21	14.1	2.4
2	12	2		−0.09	0.67	0.015	0.015	0.0018	3E-04	13	15	11.5	1.6
3	12	1	Yes	0.057	0.032	0.01	0.006	0.002	2E-04	9.5	6.2	12.6	1.2
4	12	2		0.053	0.045	0.009	0.009	0.0019	2E-04	9	8.5	12.3	1.5
5	12	3		−0.68	0.64	0.024	0.023	0.0018	4E-04	20	22	11.5	2.3
6	13	2	Yes	0.089	0.049	0.021	0.011	0.0021	3E-04	20	11	13.3	1.6
7	11	2	Yes	0.101	0.087	0.017	0.014	0.0018	2E-04	18	14	11.7	1.5
8	13	1		0.048	0.029	0.015	0.008	0.0021	2E-04	14.6	7.8	13.2	1.1
9	13	2	Yes	0.07	0.11	0.013	0.015	0.002	3E-04	11	14	12.9	2
10	13	2		0.066	0.051	0.014	0.009	0.002	2E-04	13.7	8.8	13	1.5
11	14	2		0.023	0.03	0.007	0.008	0.0021	2E-04	6.7	7.8	13.8	1.2
12	12	2		−0.03	0.6	0.016	0.02	0.0019	3E-04	14	19	12.3	2
13	13	1	Yes	0.084	0.024	0.023	0.007	0.0021	2E-04	22.4	6.6	13.7	1
14	14	2	Yes	0.055	0.078	0.007	0.011	0.0022	3E-04	6	11	14.4	1.8
15	14	3		−0.3	0.39	0.025	0.022	0.0021	4E-04	22	21	13.6	2.5
16	13	2		0.02	0.17	0.021	0.021	0.002	3E-04	18	20	13.1	2.2
17	14	2		0.053	0.032	0.014	0.009	0.0022	2E-04	13.6	8.5	13.8	1.3
18	14	1		0.05	0.022	0.014	0.006	0.0021	2E-04	13.7	5.9	13.5	1
19	15	2		0.038	0.045	0.012	0.01	0.0024	3E-04	11	10	15.1	1.8
20	15	2		0.059	0.032	0.015	0.008	0.0023	2E-04	14.2	8	14.8	1.4
21	13	2	Yes	0.05	0.14	0.017	0.014	0.002	3E-04	19	14	12.9	1.8
22				0.013	0.049	0.001	0.009	0.0023	3E-04	0.4	8.8	14.8	1.8
23	15	2		0.053	0.037	0.017	0.01	0.0023	3E-04	16	9.6	14.8	1.6
24	15	2		0.044	0.024	0.014	0.007	0.0023	2E-04	13.4	7.2	14.7	1.1
25	14	2		0.074	0.029	0.021	0.008	0.0022	2E-04	20.5	8	14	1.4
26	16	2	Yes	0.032	0.035	0.012	0.009	0.0024	2E-04	11.2	8.9	15.2	1.5
27	14	2	Yes	0.044	0.082	−0.008	0.011	0.0022	3E-04	–9	11	14	2.1
28	14	2		0.084	0.035	0.02	0.009	0.0022	2E-04	19.3	8.5	14.1	1.2
29	16	3		−0.1	0.23	0.027	0.027	0.0024	4E-04	22	25	15.5	2.3
30	15	1		0.02	0.15	0	0.024	0.0025	5E-04	–4	23	16.2	3.2
31	13	1		0.049	0.01	0.013	0.003	0.002	1E-04	13	2.5	13.1	0.5
32	14	1		0.041	0.012	0.012	0.004	0.0022	1E-04	11.6	3.6	14.1	0.8
33	14	2	Yes	0.016	0.063	0.009	0.013	0.0022	3E-04	8	13	14.1	1.8

(continued)

TABLE 4. (*contd.*)

Sample	Best age[1]	unc 2SE	PROP[2]	Common Pb Corrected	Isotopic ratios						Ages (Ma)			
					$^{207}Pb/^{206}Pb$	2SE	$^{207}Pb/^{235}U$	2SE	$^{206}Pb/^{238}U$	2SE	$^{207}Pb/^{235}U$	2SE	$^{206}Pb/^{238}U$	2SE
34	13	1		Yes	0.081	0.025	0.022	0.007	0.0021	2E-04	21.6	6.6	13.3	1
35	13	2			0.102	0.066	0.019	0.01	0.002	2E-04	18	10	12.9	1.5
36	14	1			0.054	0.011	0.015	0.003	0.0021	1E-04	15.3	3	13.5	0.6
37	14	1			0.071	0.028	0.018	0.006	0.0021	2E-04	19	6.6	13.6	1
38	13	1			0.09	0.033	0.023	0.008	0.0021	2E-04	22.2	7.8	13.5	1
39	14	2			0.077	0.045	0.018	0.01	0.0022	2E-04	17.8	9.6	14.4	1.6
40	14	2			0.075	0.039	0.022	0.012	0.0022	2E-04	21	12	14.4	1.2

*Data reduction from *Iolite geochron4*, with an Excel add-on sheet for common Pb correction and filtering.
[1]Best age is either the 206Pb/238U age or that age with a 208 based common Pb correction, after Compston *et al.* (1984).
[2]Propagated uncertainty from *Iolite* includes extra uncertainties to accommodate scatter in the data from the primary zircon reference material, Temora 2.

colours from some deposits. Samples with minimal mineral and fluid inclusions were targeted. The samples were cleaned using HNO_3, HCl, and then distilled water in an ultrasonic bath. The cleaned samples were broken into fragments in a hardened-steel percussion mill, and the fragments were picked to prepare epoxy mounts. Criteria used when selecting the samples to mount were to: (1) select the cleanest (minimal mineral inclusions and iron oxide staining) fragments; and (2) select a representation of the widest variety of colour available from each gemfield. On the basis of these criteria, 33 crystals were selected. The resin mounts were finely polished with 0.25 µm diamond solution, and they were examined with a scanning electron microscope prior to analysis.

Trace-element analyses were performed using a LA–ICP–MS at the Queensland University of Technology in two sessions. Concentrations of six elements were determined with a New Wave Excimer laser ablation system (wavelength = 193 nm) using He gas flow (0.4 L/min), coupled to an Agilent 8800 triple quadrupole ICP–MS via a junction with 1.0 L/min Ar flow in Teflon tubing. The reaction cell was idle, and the instrument was run in 'single-quad' mode. Elemental concentrations were determined by using Al_2O_3 as an internal standard and assuming that $Al_2O_3 = 98$ wt.%. The positions for spot analyses avoided inclusions, voids, edges and fractures. The ablation spot had a diameter of 85 µm, ablating at 6 Hz over 30 s laser-on time, with a laser-off period of 30 s that allowed the signal to return to background levels. Multiple spot analyses were made on each grain, and NIST 612 glass was measured between every ten spot analyses of corundum. Ablated material was carried via a He–Ar carrier gas stream to the ICP–MS, and gas blanks were measured between each analysis to determine a fitted background over the course of the analytical session. Concentrations were calculated from raw counts using NIST 612 as the external standard. Data were processed with *Iolite* (Paton *et al.*, 2011), a software package based on the calculation style of Longerich *et al.* (1996) for determination of individual concentrations and associated detection limits. Analytical precision of better than ±2% was determined by relative standard deviation (RSD%) of <2% of the measured Al in NIST 612 when those data were treated as unknowns (Pearce *et al.*, 1997). Uncertainties of one standard deviation are given for analysed elements in Table 3. High RSD in some unknowns are presumed to be the result of intracrystal variation or, possibly, microscopic

https://doi.org/10.1180/minmag.2017.081.012 Published online by Cambridge University Press

https://doi.org/10.1180/minmag.2017.081.012 Published online by Cambridge University Press

TABLE 5. Trace-element concentrations measured for Weldborough zircon megacrysts by LA–ICP–MS in ppm (*2SE*)*.

Sample	P		Ti		Y		Zr		Ce		Nd		Eu		Dy		Lu		Hf		Pb		Th		U	
1	bdl	*20*	0.51	*0.26*	189	*10*	454,000	*26,000*	0.45	*0.06*	0.02	*0.02*	0.23	*0.05*	13.67	*0.68*	8.06	*0.32*	7680	*210*	0.01	*0.01*	7.3	*0.2*	31.4	*1.4*
2	bdl	*24*	0.47	*0.26*	199	*8*	449,000	*20,000*	0.49	*0.05*	0.05	*0.04*	0.24	*0.05*	13.38	*0.57*	10.15	*0.37*	7800	*200*	0.01	*0.01*	9.8	*0.3*	39.9	*1.4*
3	1	*26*	0.38	*0.25*	257	*12*	487,000	*23,000*	0.88	*0.08*	0.07	*0.04*	0.37	*0.07*	20.55	*0.9*	10.03	*0.33*	8720	*260*	0.07	*0.02*	48.1	*1.1*	111.7	*4.6*
4	bdl	*22*	0.61	*0.26*	282	*9*	458,000	*14,000*	1.31	*0.09*	0.15	*0.07*	0.38	*0.05*	23.4	*1*	11.96	*0.42*	7980	*230*	0.05	*0.02*	25.1	*0.6*	63.8	2
5	bdl	*28*	0.33	*0.21*	135	*8*	480,000	*25,000*	0.46	*0.06*	0.02	*0.02*	0.16	*0.04*	9.19	*0.54*	5.49	*0.29*	8480	*240*	0	*0.01*	6.6	*0.2*	25.6	*1.2*
6	bdl	*28*	0.47	*0.28*	217	*11*	490,000	*25,000*	0.64	*0.06*	0.02	*0.02*	0.27	*0.05*	16.52	*0.86*	8.85	*0.31*	8350	*210*	0.03	*0.01*	18.6	*0.4*	57.2	*2.6*
7	bdl	*28*	0.39	*0.24*	252	*12*	482,000	*22,000*	0.73	*0.07*	0.07	*0.04*	0.3	*0.06*	17.81	*0.76*	13.59	*0.5*	8230	*280*	0.03	*0.02*	15.2	*0.4*	58.8	*2.3*
8	bdl	*28*	0.69	*0.32*	299	*13*	502,000	*23,000*	0.94	*0.09*	0.03	*0.03*	0.43	*0.07*	24.4	*1*	12.51	*0.34*	9420	*180*	0.04	*0.02*	41.6	*0.7*	102.1	*3.5*
9	bdl	*28*	0.64	*0.3*	212	*9*	501,000	*19,000*	0.52	*0.05*	0.01	*0*	0.23	*0.04*	14.01	*0.58*	12.16	*0.44*	9240	*200*	0.02	*0.01*	11.4	*0.2*	41.5	*1.5*
10	bdl	*28*	0.54	*0.28*	278	*10*	503,000	*20,000*	0.92	*0.08*	0.14	*0.06*	0.65	*0.07*	25.78	*0.84*	11.86	*0.34*	8820	*200*	0.03	*0.01*	31.6	*0.5*	66.9	*2.1*
11	bdl	*28*	0.6	*0.32*	316	*11*	497,000	*17,000*	0.87	*0.09*	0.08	*0.05*	0.44	*0.07*	26.86	*0.97*	12.32	*0.41*	8510	*200*	0.05	*0.02*	32.1	*0.7*	81.1	*2.4*
12	13	*28*	0.25	*0.21*	193	*7*	493,000	*18,000*	0.41	*0.06*	0.03	*0.03*	0.17	*0.04*	13.06	*0.6*	8.48	*0.3*	8620	*160*	0.01	*0.01*	10.8	*0.3*	36.4	*1.1*
13	13	*28*	0.54	*0.28*	311	*11*	492,000	*18,000*	1.07	*0.09*	0.08	*0.05*	0.5	*0.08*	27.5	*1.1*	11.23	*0.35*	8730	*210*	0.13	*0.02*	91.3	*1.8*	150.7	*4.5*
14	22	*28*	0.48	*0.25*	344	*12*	500,000	*16,000*	0.65	*0.06*	0.08	*0.05*	0.3	*0.06*	25.97	*0.99*	14.28	*0.39*	8640	*210*	0.04	*0.01*	17.7	*0.4*	63	*1.8*
15	24	*28*	0.2	*0.2*	181	*8*	497,000	*22,000*	0.35	*0.05*	0.05	*0.04*	0.18	*0.04*	13.3	*0.57*	7.42	*0.26*	9270	*180*	0.01	*0.01*	8.3	*0.2*	30.6	*1*
16	14	*28*	0.24	*0.21*	195	*7*	487,000	*16,000*	0.29	*0.04*	0.01	*0.01*	0.23	*0.04*	14.26	*0.73*	8.07	*0.26*	8820	*180*	0.02	*0.01*	9.2	*0.2*	32.9	*1*
17	19	*28*	0.08	*0.14*	250	*8*	499,000	*16,000*	0.63	*0.06*	0.09	*0.05*	0.25	*0.04*	19.8	*0.81*	9.58	*0.3*	8930	*200*	0.05	*0.02*	37.7	*0.7*	84.5	*2.3*
18	bdl	*28*	0.18	*0.16*	277	*9*	495,000	*15,000*	0.84	*0.07*	0.07	*0.05*	0.41	*0.06*	22.51	*0.86*	10.46	*0.34*	8780	*180*	0.09	*0.02*	68.9	*1.2*	127.1	*3.2*
19	26	*28*	0.46	*0.23*	196	*6*	501,000	*16,000*	0.52	*0.05*	0.02	*0.02*	0.23	*0.06*	13.71	*0.56*	7.47	*0.29*	9020	*170*	0.04	*0.02*	25.9	*0.5*	67.9	*1.7*
20	29	*28*	0.31	*0.21*	356	*13*	502,000	*20,000*	0.93	*0.08*	0.12	*0.06*	0.46	*0.07*	30.3	*1.1*	14.32	*0.37*	8310	*180*	0.04	*0.02*	34.6	*0.6*	86.4	*2.5*
21	28	*28*	0.57	*0.24*	365	*13*	489,000	*14,000*	0.82	*0.07*	0.16	*0.07*	0.54	*0.08*	31.66	*0.94*	12.58	*0.45*	6970	*150*	0.02	*0.01*	12.1	*0.3*	46.7	*1.3*
22	13	*28*	0.53	*0.29*	424	*14*	482,000	*17,000*	0.98	*0.07*	0.16	*0.06*	0.61	*0.08*	34.7	*1.2*	15.48	*0.48*	6220	*140*	0.03	*0.01*	12.1	*0.3*	56.6	*1.7*
23	6	*28*	0.53	*0.26*	388	*11*	480,000	*13,000*	1.06	*0.09*	0.18	*0.07*	0.78	*0.09*	36.3	*1.1*	11.49	*0.33*	6150	*140*	0.03	*0.01*	19.8	*0.4*	68.4	*1.4*
24	1	*28*	0.45	*0.24*	387	*12*	493,000	*16,000*	1.29	*0.1*	0.2	*0.07*	0.78	*0.1*	38.8	*1.6*	11.26	*0.41*	6230	*150*	0.06	*0.02*	41.6	*0.9*	107.9	*2.8*
25	bdl	*28*	0.27	*0.22*	406	*11*	484,000	*13,000*	1.47	*0.11*	0.25	*0.07*	0.79	*0.08*	39.1	*1.1*	12.6	*0.41*	6490	*150*	0.05	*0.02*	46.8	*0.9*	107.6	*2.3*
26	13	*28*	0.66	*0.27*	469	*12*	495,000	*13,000*	1.33	*0.09*	0.15	*0.06*	0.96	*0.1*	46.4	*1.7*	14.24	*0.45*	6580	*140*	0.02	*0.02*	25.4	*0.5*	78.3	*1.4*
27	30	*28*	0.39	*0.26*	273	*7*	500,000	*13,000*	0.63	*0.06*	0.08	*0.04*	0.41	*0.06*	22.2	*1*	9.01	*0.33*	6760	*130*	0.01	*0.01*	7.3	*0.2*	37.21	*0.86*
28	3	*28*	0.43	*0.29*	316	*8*	498,000	*13,000*	0.99	*0.08*	0.09	*0.06*	0.58	*0.07*	29.1	*1.1*	9.99	*0.36*	6750	*150*	0.03	*0.01*	28.9	*0.6*	82	*1.8*
29	6	*28*	0.68	*0.27*	228	*9*	497,000	*18,000*	0.44	*0.06*	0.08	*0.05*	0.35	*0.05*	17.69	*0.82*	7.5	*0.29*	6410	*130*	0.01	*0.01*	6	*0.1*	29.74	*0.79*
30	19	*28*	0.36	*0.3*	211	*7*	499,000	*18,000*	0.39	*0.05*	0.04	*0.03*	0.28	*0.05*	17.03	*0.74*	6.5	*0.26*	6650	*130*	0.01	*0.01*	4	*0.1*	22.23	*0.6*
31	33	*28*	0.24	*0.18*	169	*5*	485,000	*15,000*	0.47	*0.05*	0.11	*0.04*	0.43	*0.06*	15.57	*0.74*	6.17	*0.27*	10360	*240*	0.23	*0.03*	176.3	*3.8*	459	*11*
32	28	*28*	0.05	*0.15*	172	*7*	496,000	*21,000*	0.43	*0.06*	0.09	*0.04*	0.51	*0.08*	15.09	*0.68*	6.45	*0.26*	9600	*270*	0.17	*0.02*	115.6	*2.4*	293.6	*9.4*
33	25	*28*	0.04	*0.15*	60	*2*	509,000	*16,000*	0.09	*0.02*	0.01	*0*	0.03	*0.02*	1.5	*0.23*	1.38	*0.16*	10910	*230*	0	0.01	9.3	0.3	44.5	1.6
34	27	*28*	0.6	*0.29*	201	*13*	482,000	*17,000*	0.18	*0.03*	0.01	*0.02*	0.15	*0.03*	13.8	*1.5*	10.07	*0.54*	8670	*230*	0.06	*0.02*	39.7	*3.9*	196	*13*
35	21	*28*	0.21	*0.2*	81	*3*	493,000	*18,000*	0.1	*0.03*	0.01	*0*	0.09	*0.03*	3.65	*0.29*	2.86	*0.17*	10030	*260*	0.02	*0.01*	15.8	*0.4*	71.3	*1.9*
36	bdl	*28*	0.5	*0.32*	210	*8*	495,000	*18,000*	0.5	*0.05*	0.11	*0.05*	0.39	*0.07*	17.04	*0.68*	8.74	*0.29*	10520	*240*	0.16	*0.02*	137.4	*3*	389	*12*
37	9	*28*	0.28	*0.23*	108	*4*	492,000	*17,000*	0.22	*0.03*	0.02	*0.02*	0.15	*0.04*	6.94	*0.43*	4.39	*0.17*	10910	*220*	0.04	*0.02*	35.8	*0.7*	155.5	*3.9*
38	14	*28*	0.21	*0.19*	95	*4*	498,000	*17,000*	0.14	*0.02*	0.01	*0.02*	0.09	*0.03*	5.22	*0.4*	3.66	*0.19*	11480	*260*	0.03	*0.01*	26.3	*0.5*	125.8	*3.4*
39	bdl	*28*	0.06	*0.16*	83	*3*	500,000	*16,000*	0.14	*0.03*	0.02	*0.02*	0.07	*0.02*	4.03	*0.3*	3.12	*0.14*	10690	*230*	0.01	*0.01*	17.3	*0.4*	77	*2.3*
40	bdl	*28*	0.28	*0.21*	84	*3*	501,000	*19,000*	0.12	*0.03*	0	*0.01*	0.09	*0.03*	3.83	*0.25*	3.34	*0.16*	10930	*250*	0.02	*0.01*	17.7	*0.3*	80.3	*2.5*

Data for La are not shown as they were all below the detection limit.

*Data reduction from *Iolite Trace Elements IS*. Trace-element concentrations assume a stoichiometric Si content of 15.32 wt.% Si.

mineral/melt inclusions. Detection limits for the analysed elements are in Supplementary Table 1 which has been deposited with the Principal Editor of *Mineralogical Magazine* and is available from http://www.minersoc.org/pages/e_journals/dep_mat_mm.html

Additionally, four dark–red zircon crystals (3–5 mm in diameter), fossicked with alluvial sapphires from Weldborough, were mounted in epoxy, ground to expose cores and polished. Each of these crystals was analysed 10 times with LA–ICP–MS. Groups of five measurements of unknowns were bracketed by standards, resulting in 12 measurements of each standard, given extra sets ablated at the beginning and end of the session. The isotopes analysed were ^{29}Si, ^{31}P, ^{49}Ti, ^{57}Fe, ^{89}Y, ^{91}Zr, $^{206–208}$Pb, ^{232}Th and ^{238}U, plus six rare-earth elements (*REE*s). Only the 'essential' *REE*s were collected to save analytical time in an already long list of elements, given that geochronology was the main objective. The zircon crystals were ablated using a 30 μm beam with a lab setup similar to that described above, using the *Iolite Geochronology 4* routine. Robust ages are taken to be those that are concordant within stated uncertainties for those crystals. Temora 2 zircons ($n = 12$; Black *et al*., 2004) were used as the primary standard and Plešovice zircons as the monitor standard. Plešovice zircons yielded an age of 325 ± 8 Ma for 12 analyses, a result comparable to its accepted TIMS age of 337.13 ± 0.37 Ma (Sláma *et al*., 2008). Raw data were processed using *Iolite* (Paton *et al*., 2011), and population weighted average ages were calculated using the *Isoplot 3.7* toolkit (Ludwig, 2008). Common Pb corrections and trace-element compositions were determined with Excel spreadsheets, as provided in Tables 4 and 5. The trace-element standard NIST 610 was used, and Si was used as an internal standard. A silica composition of $SiO_2 = 32.8$ wt.% (stoichiometric) was assumed.

Results

Trace-element concentrations of corundum

Concentrations of Mg, Ti, V, Cr, Fe and Ga (the most important trace elements in corundum for genetic classification) were determined with LA–ICP–MS as described in Table 3. The isotopes measured were ^{24}Mg, ^{27}Al, ^{49}Ti, ^{51}V, ^{52}Cr, ^{57}Fe and ^{71}Ga. Corundum crystals analysed for this study contain greater concentrations of chromophore

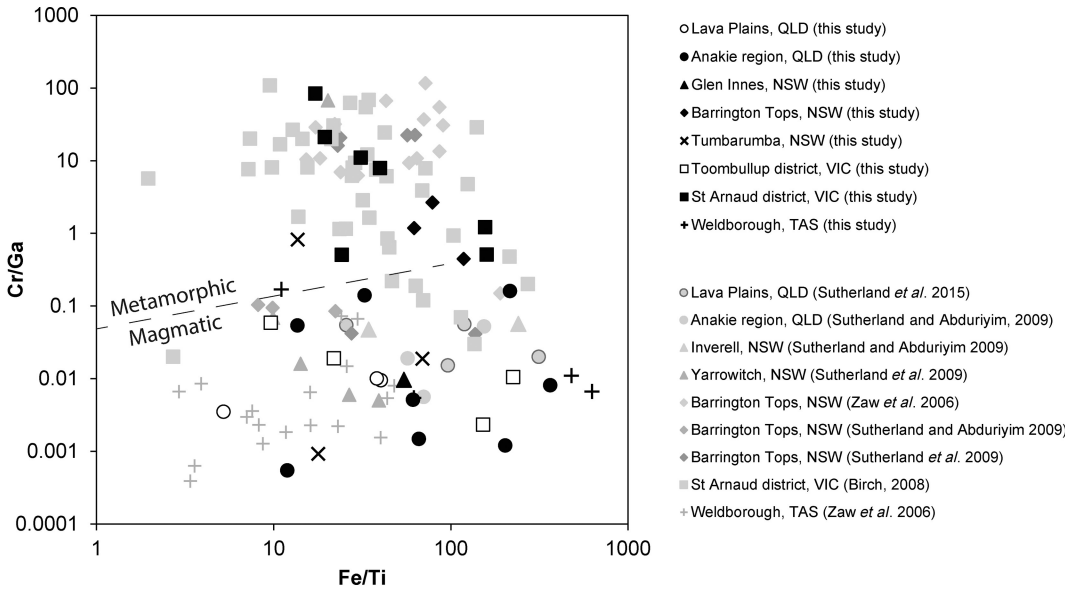


FIG. 4. Trace-element ratios from LA–ICP–MS results for all corundum samples of Fe/Ti plotted against Cr/Ga, after Sutherland *et al*. (1998*b*). Comparisons of data from Birch (2008), Sutherland and Abduriyim (2009), Sutherland *et al*. (2009), Sutherland *et al*. (2015) and Zaw *et al*. (2006) are underlain in grey symbols.

https://doi.org/10.1180/minmag.2017.081.012 Published online by Cambridge University Press

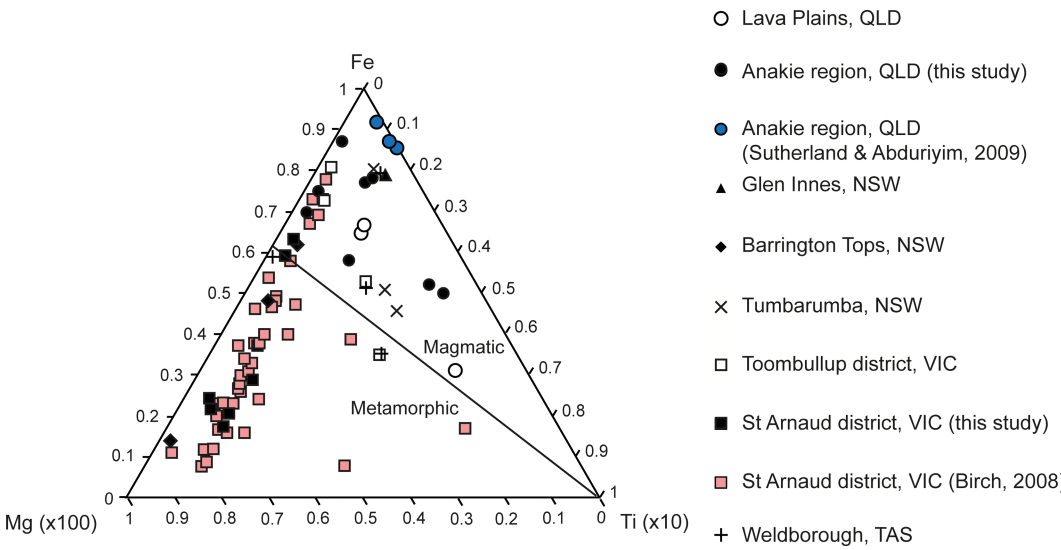


FIG. 5. Comparisons between our data, Birch (2008) and Sutherland and Abduriyim (2009) shown by an Fe-Mg-Ti ternary plot after Peucat *et al*. (2007). Division between magmatic and metamorphic sapphires are also from Peucat *et al*. (2007). Blue and pink fillings highlight comparative studies; colour filling does not represent the corundum colour.

elements such as Fe (2055–10,202 ppm; $\mu = 5753$ ppm), Cr (1.5–4367 ppm; $\mu = 392$ ppm), Ti (7–1952 ppm; $\mu = 202$ ppm) and V (2.2–73 ppm; $\mu = 20$ ppm) than non-chromophore elements such as Mg (1.5–236 ppm; $\mu = 58$ ppm) and Ga (17–390 ppm; $\mu = 132$ ppm). An outlier of 621 ppm for Mg has been excluded for a better representation of Mg concentrations. Regardless of some relatively high Cr concentrations, there were 21 spots that had Cr concentrations below detection limits (average detection limit of Cr is 1.24 ppm). Other detection limits (shown as averages) were Mg (0.40 ppm), Ti (1.19 ppm), V (0.15 ppm), Fe (19.67 ppm) and Ga (0.35 ppm). Multiple spot analyses were conducted on each crystal, and when calculating the mean concentration for the sample, half of the detection limit was used for concentrations that were below the detection limit. Calculated mean concentrations, standard deviations and RSD% for the 33 crystals are in Table 3. Note that the range of total measured trace-element ($n = 6$) concentrations in our samples (assuming 98 wt.% Al_2O_3) is 2230–15,000 ppm (~0.4–3 wt.% oxide).

Trace-element data for corundum from eastern Australia display a continuum between Fe/Ti, Cr/Ga and Ga/Mg, as well as trace-elemental ternary plots (Figs 4–7). On plots of Fe/Ti *vs.* Cr/Ga, sapphires from Lava Plains, the Anakie region, Glen Innes and the Toombullup district would be previously classified as magmatic corundum; sapphires from Tumbarumba and Weldborough are both magmatic and metamorphic; and sapphires and rubies from Barrington Tops and St Arnaud district are metamorphic (Fig. 4). On ternary plots of Fe, Ti and Mg, sapphires from Lava Plains, Tumbarumba, the Anakie region and Glen Innes would be classified as magmatic corundum, while sapphires and rubies from the Barrington Tops, Toombullup district, St Arnaud district and Weldborough fall along a transition between metamorphic and magmatic corundum (Fig. 5). Plots of Ga/Mg *vs.* Fe illustrate that Australian alluvial sapphires do not fall in the pre-defined region of 'metamorphic sapphires' (Fig. 7*a*). On the basis of Ga/Mg and Fe/Mg, sapphires from Lava Plains, Glen Innes and Weldborough would be classified traditionally as magmatic; sapphires from the Anakie region, Tumbarumba and Toombullup district would be classified as magmatic to metasomatic; and sapphires and rubies from Barrington Tops and the St Arnaud district would be classified as metamorphic (Fig. 7*b*). In summary, on the basis of the different trace-element classifications outlined above from data generated in one laboratory during two sessions, the only consistent classification is for sapphires from the Lava Plains gemfield, which are classified as 'magmatic' regardless of trace-element ratio.

https://doi.org/10.1180/minmag.2017.081.012 Published online by Cambridge University Press

Ages of alluvial zircons from the Weldborough field

Thirty-nine of the forty ablated points from the Weldborough zircons are concordant within uncertainty, but the uncertainties on $^{207}Pb/^{235}U$ are large because of the relatively young age and low U concentration (average = 97 ± 92 ppm). The weighted mean age for the Weldborough zircons is 13.61 ± 0.3 Ma (MSWD = 1.3), including nine ages that were common-Pb corrected using a ^{208}Pb-based correction (see Fig. 8; Table 4). At this age level, a correction for Th disequilibria is negligible and has not been conducted. The Weldborough zircons are outstanding in having a very low (subsolidus?) calculated *T* from Ti content (Watson *et al*., 2006), assuming a Ti activity of 1. The average temperature is 511 ± 35°C (average Ti content of 0.4 ppm). Lower assumed activities could increase this average *T* by some 50°C, but it is still a very low calculated temperature of crystallization. For comparison, Plešovice zircons yielded crystallization temperatures of 945 ± 44°C, and Temora zircons 714 ± 24°C. Furthermore, the Weldborough zircons have very low trace-element concentrations, as shown in Table 5. Phosphorus averaged 14 ppm, with half the population below the detection limit. Average Th content was 34 ± 37 ppm, U content was 97 ± 92 ppm, Y content was 242 ± 102 ppm and Lu was 9 ± 4 ppm. The *REE* concentrations of Weldborough zircons are generally less than those of most eastern Australian zircons, but they have similar *REE* patterns (Fig. 9). Another unusual feature in the Weldborough zircons, apart from low *REE* concentrations, is that Zr/Hf averages 59 ± 11, a relatively high value given a range of 30–60 for igneous zircons (Claiborne *et al*., 2006).

Discussion

The formation of corundum is a matter of considerable debate, but the processes of magmatism, metasomatism and metamorphism are all probably involved. Many previous studies have used geochemical data to subdivide corundum into distinct compositional groups (e.g. Sutherland *et al*., 1998*b*, 2009; Garnier *et al*., 2005; Abduriyim and Kitawaki, 2006; Zaw *et al*., 2006; Peucat *et al*., 2007; Sutherland and Abduriyim, 2009). In contrast, our new data illustrate a spectrum of trace-element compositions (Figs 4–7), suggesting similar but varying geochemical

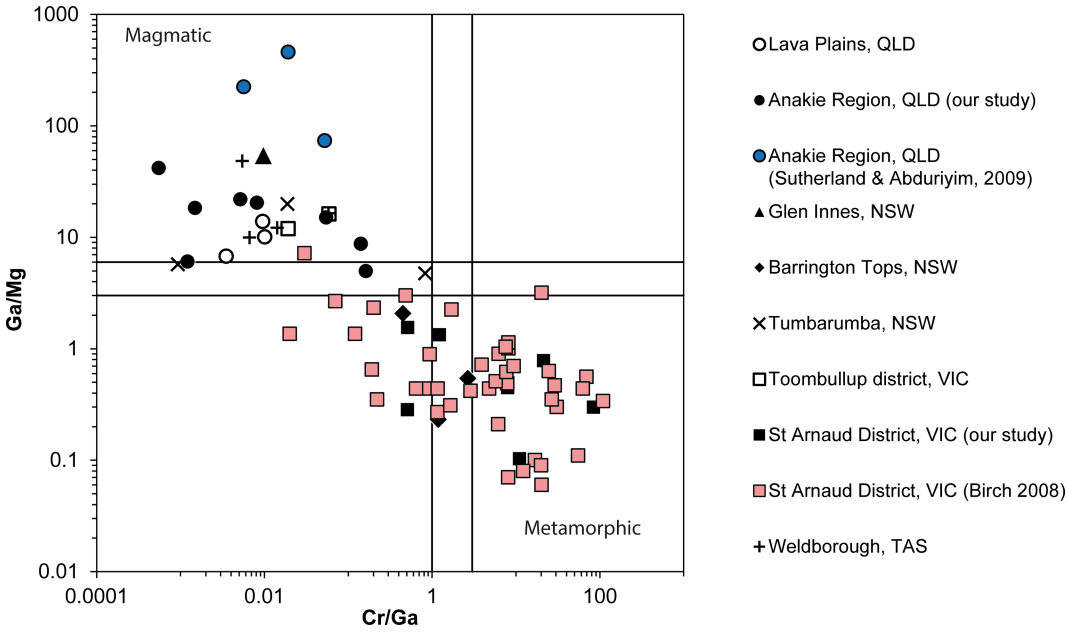


FIG. 6. Comparisons between our data, Birch (2008) and Sutherland and Abduriyim (2009) in a Cr/Ga *vs.* Ga/Mg diagram. Boundaries between magmatic and metamorphic sapphires are from Sutherland *et al*. (1998*b*) and Sutherland *et al*. (2015). Blue and pink fillings highlight comparative studies; colour filling does not represent the corundum colour.

https://doi.org/10.1180/minmag.2017.081.012 Published online by Cambridge University Press

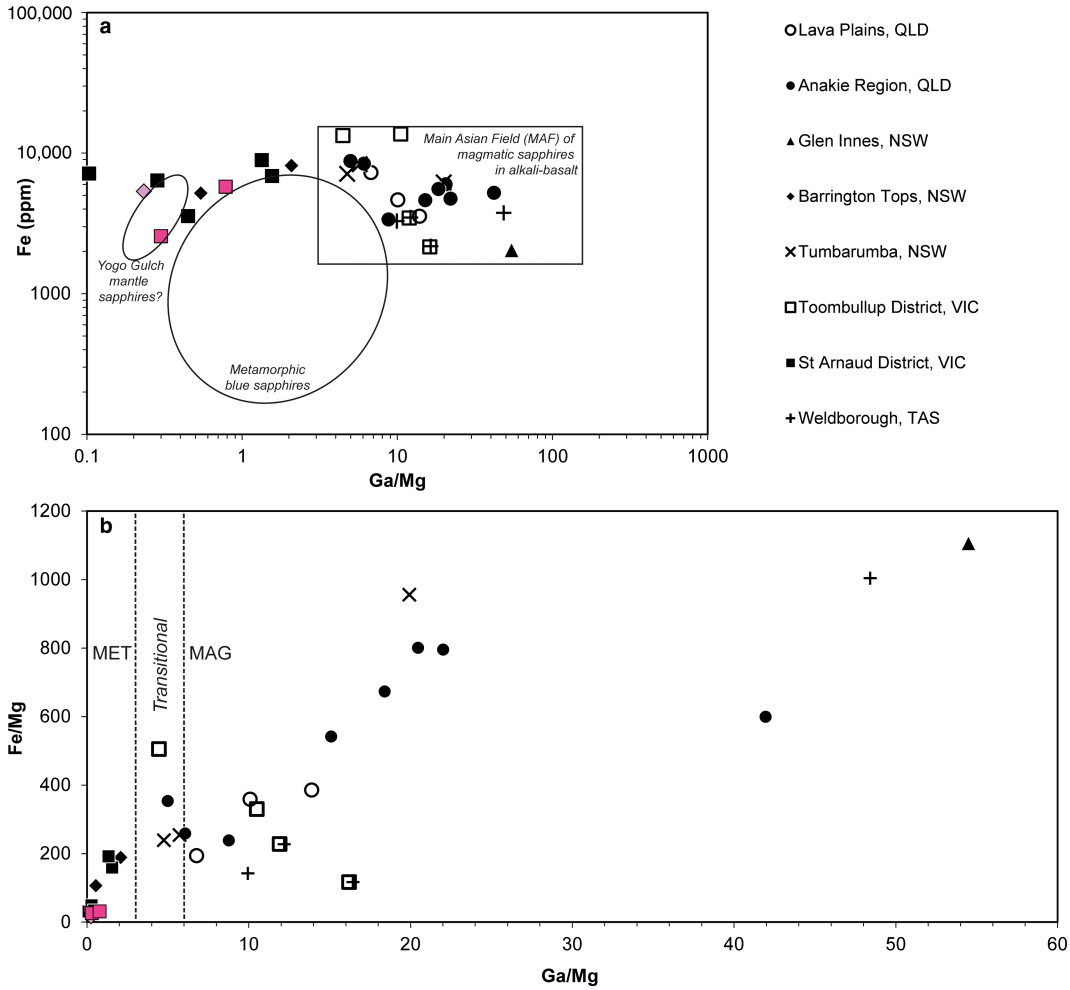


FIG. 7. Eastern Australian corundum Ga/Mg plots: (*a*) Ga/Mg *vs*. Fe (ppm) from Peucat *et al*. (2007); the outlined regions are from Peucat *et al*. (2007); (*b*) Ga/Mg *vs.* Fe/Mg from Sutherland *et al*. (2015). Pink squares represent ruby samples and the pink diamond represents a pink sapphire.

parentage of the sapphires and rubies from eastern Australia. Geochemical variation plots (Fig. 10) demonstrate the difficulty in distinguishing between igneous and metasomatic origins for Australian alluvial sapphires, whereas rubies are more distinct, and seem to be derived from ultramafic metamorphic rocks on the basis of the geochemical variation plot (Fig. 10). Our findings therefore suggest that trace-element boundaries do not definitively distinguish 'magmatic', 'metasomatic' and 'metamorphic' corundum from basalt-hosted deposits. In particular, the St Arnaud district has a large proportion of sapphires and rubies of intermediate composition. We compare our new data from the St Arnaud district with previous data from Birch (2008; Figs 5 and 6). Both datasets illustrate a continuum in trace-element compositions between Fe- and Mg-rich end-members in St Arnaud corundum (Fig. 5). Importantly, there is no gap between $Fe_{0.5}$ and $Fe_{0.7}$, a gap that has been used as a basis for distinguishing 'magmatic' and 'metamorphic' blue sapphires from a number of locations in SE Asia and Africa (Peucat *et al*., 2007). Similarly, Figs 4 and 6 illustrate a continuous compositional spectrum in eastern Australian sapphires in terms of Ga/Mg and

https://doi.org/10.1180/minmag.2017.081.012 Published online by Cambridge University Press

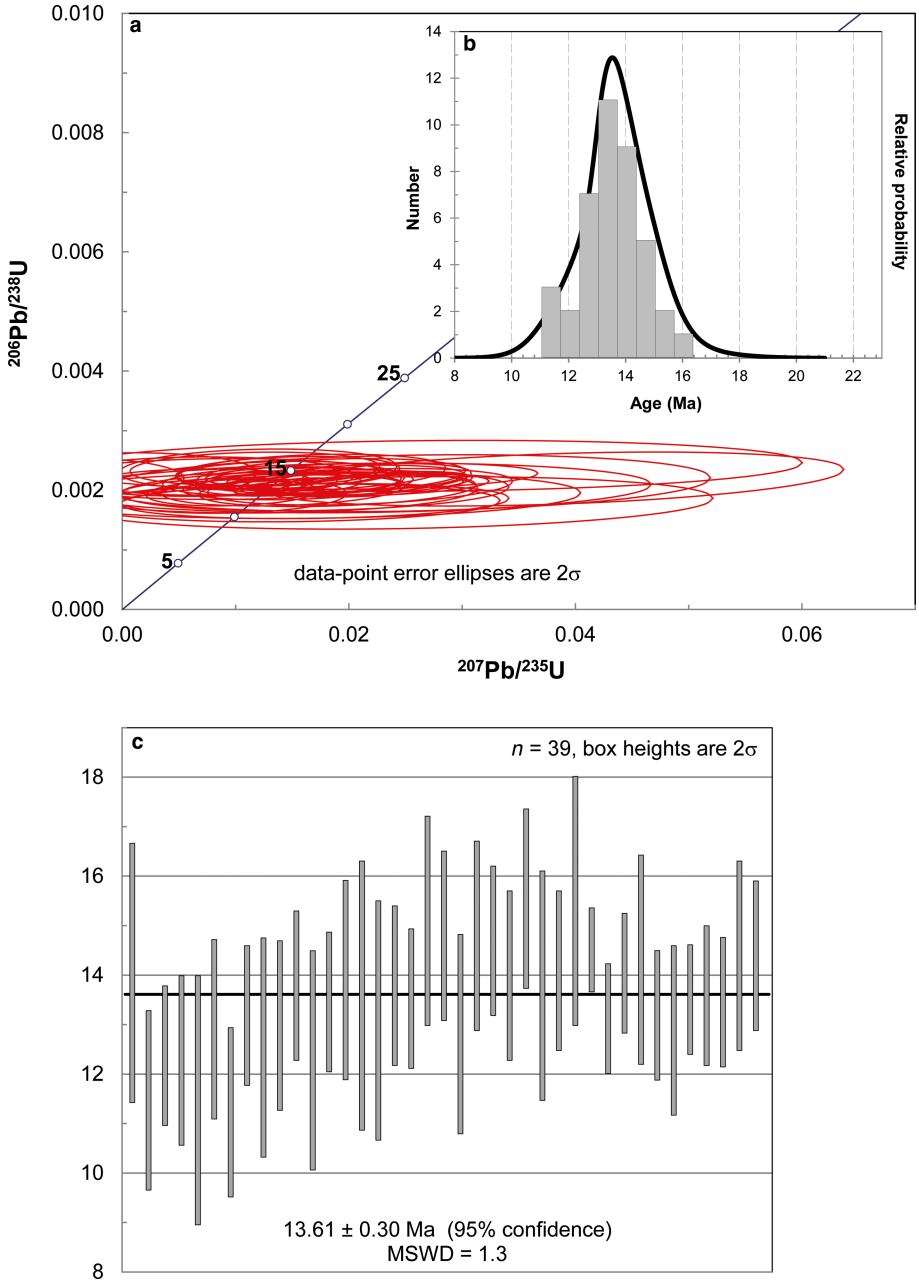


FIG. 8. U–Pb age of Weldborough zircon megacrysts. (*a*) Conventional U–Pb Concordia plot following Wetherill (1956) with an inset figure of (*b*) $^{206}Pb/^{238}U$ age histogram; (*c*) Mean-weighted average plot.

Cr/Ga. The continuum suggests that there is little reason to ascribe definitive compositional boundaries between magmatic and metamorphic corundum.

Heterogeneity in corundum composition

Compositional zonation, which has been observed previously in many corundum crystals (e.g. Zaw

https://doi.org/10.1180/minmag.2017.081.012 Published online by Cambridge University Press

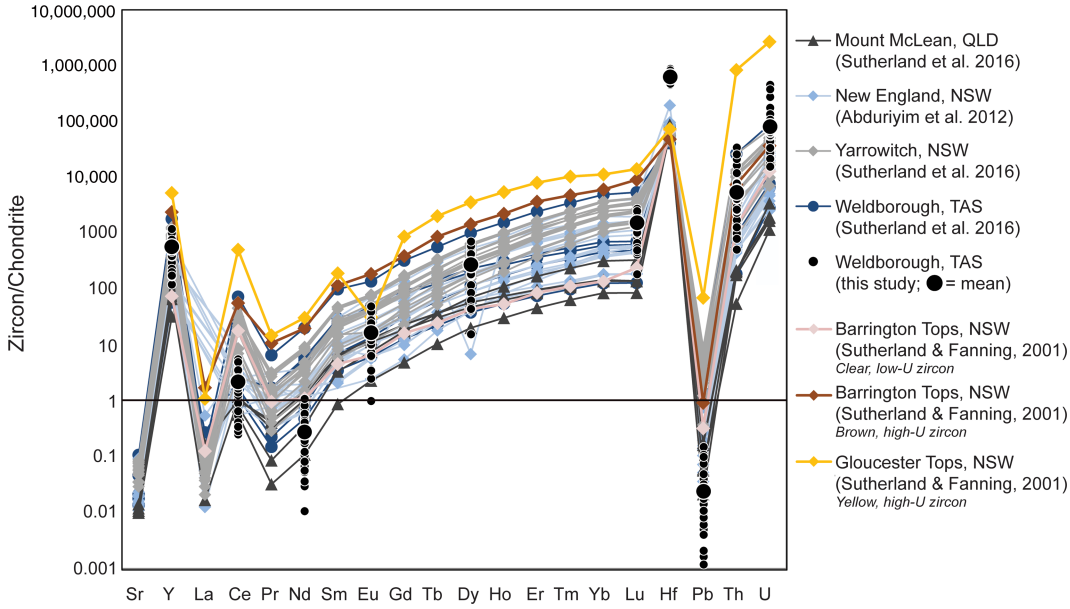


FIG. 9. Chondrite-normalized *REE* diagram comparing zircon megacrysts from Weldborough, Tasmania (this study) with zircon megacrysts from QLD, NSW and TAS from Abduriyim *et al*. (2012), Sutherland and Fanning (2001) and Sutherland *et al*. (2016).

et al., 2006), may be partially responsible for the range of trace-element compositions illustrated in Figs 4–7. Zonation can appear in different forms, such as trapiche rubies and sapphires (e.g. Garnier *et al*., 2002; Sutherland *et al*., 2002) or colour-zoning (e.g. Sutherland and Coenraads, 1996; Sutherland *et al*., 2008). 'Magmatic' sapphires are commonly growth-zoned (Sutherland *et al*., 1998*b*); zoning is also observed in 'metamorphic' rubies (Harlow and Bender, 2013). Titanium concentrations vary from core to rim in some Australian 'magmatic' alluvial corundum (Zaw *et al*., 2006; Sutherland *et al*., 2009), and Australian 'metamorphic' alluvial corundum vary core to rim in Cr and Fe (Sutherland *et al*., 2009). Given that the reference material, NIST612 glass, had RSD% within 2%, we interpret the relatively high RSD% for some multiple spot measurements of trace-element concentrations within single-crystal fragments (e.g. Ti in D816-003, Mg and Fe in D43427-009; Table 3) as caused by geological zonation. One plausible mechanism for generating such zonation is from corundum crystallizing in a differentiating magma. Trace-element gradients from core to rim may reflect gradual changes in the composition of the crystallizing melt (e.g. Zaw *et al*., 2006), and magma differentiation might be a key and largely overlooked process affecting corundum composition.

Associated zircon megacrysts ages: new findings from northeast Tasmania

The U–Pb ages from zircon inclusions within corundum, as well as from zircon megacrysts found alongside detrital corundum in eastern Australian gemfields (Fig. 3), provide an additional clue about the formation of eastern Australian corundum. Although as old as ~900 Ma, most of the zircons in corundum are ~3–50 Ma, roughly the same age as the host lava-fields, suggesting that lava-field magmatism was important not only for the transportation of corundum to the surface, but also to the formation of corundum (and zircon). The Weldborough gemfield in NE Tasmania includes both sapphires and zircon megacrysts, and it is associated spatially with Weldborough basalt (~47 Ma) and Ringarooma Valley basalts (13–16 Ma; McGee, 2005). Some Weldborough sapphires have zircon inclusions with ages that match the Weldborough basalt age of 46.8 Ma (Sutherland and Wellman, 1986; McGee, 2005), though some zircon megacrysts from Weldborough have Triassic U–Pb ages (Zaw *et al*., 2006). Our new U–Pb results

https://doi.org/10.1180/minmag.2017.081.012 Published online by Cambridge University Press

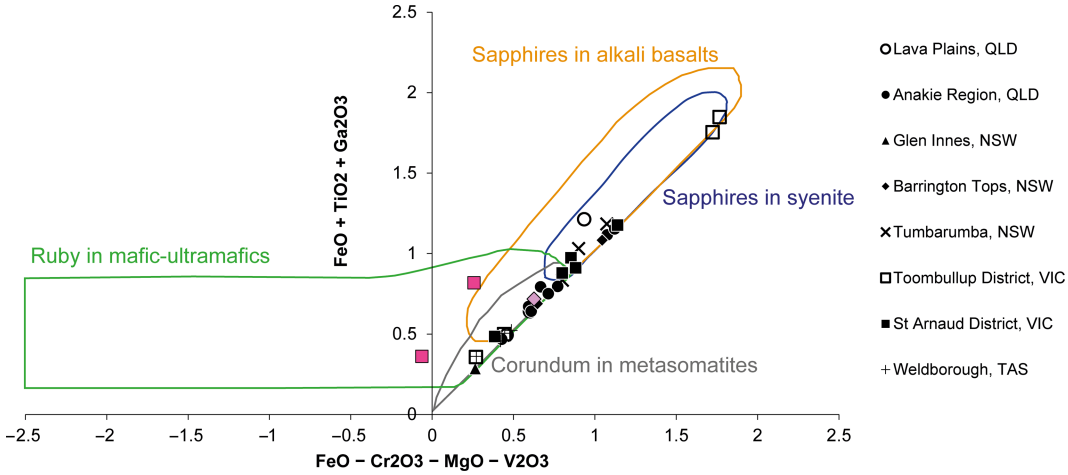


FIG. 10. Compositional variations of corundum megacrysts from eastern Australia in the $FeO–Cr_2O_3–MgO–V_2O_3$ *vs*. $FeO+TiO_2+Ga_2O_3$ (in wt.%) classification diagram (Giuliani *et al*., 2014). Pink squares represent ruby samples and the pink diamond represents a pink sapphire.

document a young age of ~13.61 ± 0.3 Ma for zircon megacrysts from the Weldborough region. The age of zircons from our study matches the age of the youngest phase of volcanism (13–16 Ma) in the nearby Ringarooma–Winnaleah area of NE Tasmania (Sutherland and Wellman, 1986). It was previously concluded by McGee (2005) that the ~47 Ma Weldborough basalt is the only source of alluvial sapphires and zircons in the Weldborough region, but our new data suggest that the Ringarooma Valley basalts are also a source for sapphires and zircons in this area. We conclude, therefore, that the sapphires and zircons from the Weldborough area have a variety of sources. Sapphires with zircon inclusions that are ~47 Ma are clearly related to the Weldborough basalt (McGee, 2005), zircon megacrysts from this study that are ~13.6 Ma are associated with the comparatively young Ringarooma basalt, and Triassic zircon megacrysts ages (Zaw *et al*., 2006) are associated with a third, somewhat enigmatic source. Our trace-element data from the mid-Miocene Weldborough zircon megacrysts thus bear on the youngest known phase of gemstone formation in the region.

The trace-element pattern in the young Weldborough zircon megacrysts fits within the majority of eastern Australian zircon megacrysts, though it differs slightly. Three key features of Weldborough zircons megacrysts from this study are high Zr/Hf (59 ± 11), low crystallization temperature (511°C) and low *REE* concentrations. Zr/Hf greater than the chondritic value commonly arise from continental and oceanic intraplate volcanism (Dupuy *et al*., 1992), but those that are very high are associated with partial melting of metasomatized mantle (Kogarko, 2016*a*, 2016*b*). On the basis of Ti concentrations, igneous zircons globally have crystallization temperatures ranging from 500 to 850°C (Fu *et al*., 2008), and the Weldborough zircons fall into the lowest part of this range (511 ± 35°C). Low temperatures could be related to hydrothermal processes (Schaltegger, 2007), but the Weldborough zircons lack *LREE* enrichment (Hoskin, 2005) that would be suggestive of a hydrothermal source. Low total *REE* concentrations reflect ultramafic and alkaline source compositions (Belousova *et al*., 2002).

The Weldborough zircons are most similar to a low-U zircon megacryst from Barrington (Sutherland and Fanning, 2001) and a pale brown zircon from Boat Harbour, NNW Tasmania (Sutherland, 1996). A model for the formation of zircon megacrysts that fits with the observed *REE* patterns from this study is crystallization from a mantle melt derived from partial melting of a metasomatized mantle (Sutherland, 1996). Examples of zircons with similar *REE* patterns outside of Australia include corundum-bearing syenitic xenoliths from Ilmen, Russia (Hinton and Upton, 1991) and zircon syenite pegmatites in Italy (Stähle *et al*., 1990).

https://doi.org/10.1180/minmag.2017.081.012 Published online by Cambridge University Press

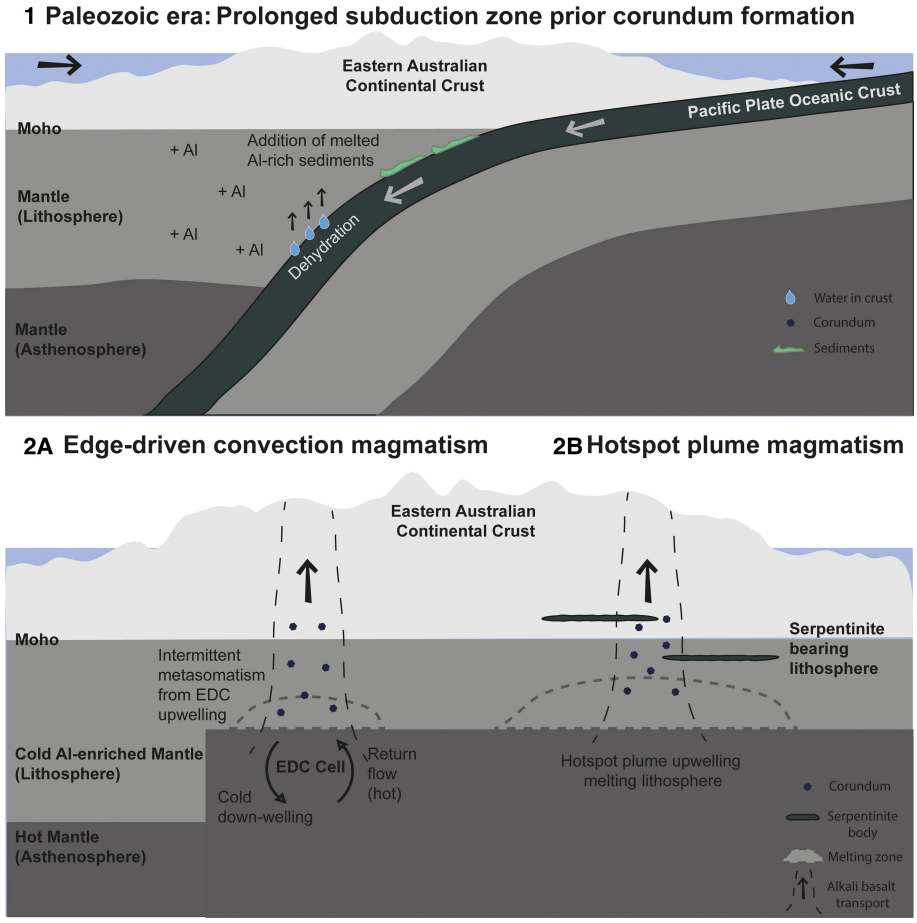


FIG. 11. Schematic diagram of (1) Paleozoic west-dipping subduction that enriches the mantle wedge with Al and volatiles, then (2) two modes of generating intraplate volcanism in eastern Australia from Mesozoic until recent times, which transport gem corundum and zircon megacrysts from the mantle and/or crust to the surface; (2A) represents edge-driven convection proposed by Fishwick *et al*. (2008) and Davies *et al*. (2015), whereas (2B) represents a hotspot model proposed by Sutherland *et al*. (1998*a*). The model also incorporates the potential interaction with serpentinite belts to form corundum in 2B (Sutherland and Fanning, 2001; Sutherland *et al*., 2002).

A potential subduction zone component in the formation of eastern Australian alluvial corundum

Given the long Paleozoic–Mesozoic history of subduction beneath eastern Australia (e.g. Glen, 2005; Fergusson and Henderson, 2015), subduction was potentially an important process in creating Al-enrichment in the mantle wedge beneath eastern Australia, which later facilitated corundum formation. Sediment contributions from prolonged subduction would have added Al and volatiles to the mantle wedge by melting of Al-rich sediments on the oceanic crust. Our findings suggest that mixing processes or interaction between sources were key to resultant corundum trace-element compositions. Al-rich magmas might have been generated from pre-conditioned lithospheric mantle that later interacted with the lower crust, creating mixed geochemical signatures in corundum (Fig. 11). These interactions have been proposed for deposits from other continents (Sutherland *et al*., 1998*a*; Yui *et al*., 2003; Garnier *et al*., 2005; Palke *et al*., 2016). In the Anakie region, New England, Yarrowitch, Barrington Tops, Tumbarumba and Weldborough

https://doi.org/10.1180/minmag.2017.081.012 Published online by Cambridge University Press

gemfields, corundum has mantle-like $\delta^{18}O$ ranging from 3.6‰ to 6.5‰ (Zaw *et al*., 2006; Sutherland *et al*., 2009). This range is typical of mantle eclogites and serpentinites (Bindeman *et al*., 2005), and reactions involving ultramafic to mafic Cr-bearing serpentinite bodies have been suggested as important processes in corundum crystallization (e.g. in Australian fold belts; Sutherland and Fanning, 2001; Sutherland *et al*., 2002). In fact, serpentinite bodies occur in the vicinity of the Lava Plains, Glen Innes, Barrington Tops and Tumbarumba districts, an association that speaks to a connection between corundum formation and subduction zone processes that existed in eastern Australia for much of the Phanerozoic. We suggest that subduction preconditioning is important in creating an Al-enriched mantle wedge that, when tapped by subsequent intraplate basaltic volcanoes, gives rise to corundum and zircon crystallization. This general process would explain many features of the eastern Australian gemstone belt: mantle-like $\delta^{18}O$ for many Australian sapphires and zircons; the spatial and temporal correspondence with Cenozoic intraplate mafic magmatism; and the spatial correspondence with a long-lived subduction zone.

In short, the great accumulation of corundum in eastern Australia may owe its existence to the combination of what are arguably the two most important aspects of the Phanerozoic tectonic history of the region: Paleozoic–Mesozoic west-dipping subduction, followed by Mesozoic–Cenozoic basaltic magmatism that was generally related to the opening of the Tasman and Coral seas. Our reasoning suggests that not only are previous subduction zones crucial for ruby formation, as emphasized by Sutherland and Fanning (2001) and Sutherland *et al*. (2002), they are also important, in some cases, for the formation of sapphires.

Conclusions

This is the first study to incorporate Australian gemfields in Victoria into a regional study of eastern Australian sapphire and ruby, thus providing a more diverse and comprehensive database of corundum trace-element compositions than previously assembled. Trace-element data from these gemfields were collected in the same laboratory, removing the complication of interlaboratory analytical variations in data comparison. Trace-element concentrations and ratios from eastern Australian corundum define a continuous trend between end-member compositions that have been traditionally referred to as 'magmatic' and 'metamorphic' (Sutherland *et al*., 1998*b*; Peucat *et al*., 2007). This variation may arise from magma differentiation, magma mixing, or assimilation-fractional crystallization processes, as well as metamorphic and metasomatic processes. Previous $\delta^{18}O$ data from eastern Australian alluvial sapphire and ruby suggest a mantle source, with minor contributions from crustal material that could have been subducted sediment or crust underlying eastern Australian lava-fields. The location of the eastern Australian gemstone belt in proximity to an ancient and long-lived subduction zone suggests that metasomatism of the mantle wedge is an important factor in the formation of basalt-related corundum.

Acknowledgements

The authors thank Dr. William Birch from Victoria Museum, Kristen Spring and Andrew Rozefelds from Queensland Museum, and Ross Pogson from Australian Museum for their generous donations of corundum samples. The authors acknowledge the facilities and the scientific and technical assistance of the Australian Microscopy and Microanalysis Research Facility at the UQ Centre for Microscopy and Microanalysis, as well as the Central Analytical Research Facility at the Queensland University of Technology. They also thank Karine Moromizato from QUT for assistance with *Iolite* software, Isabelle Jones (UQ) and Tracey Crossingham (UQ) for helpful discussions about Cenozoic mafic magmatism in eastern Australia and Aaron Palke (UQ and Queensland Museum) for reading the manuscript and providing important feedback. They are grateful to the anonymous reviewers for their critical comments that helped to improve the original manuscript and the Associate Editor Stuart Mills for handling the manuscript.

References

Abduriyim, A. and Kitawaki, H. (2006) Applications of laser ablation-inductively coupled plasma-mass spectrometry (LA-ICP-MS) to Gemology. *Gems and Gemology*, **42**, 87–108.

Abduriyim, A., Sutherland, F.L. and Belousova, E.A. (2012) U-Pb age and origin of gem zircon from the New England sapphire fields, New South Wales, Australia. *Australian Journal of Earth Sciences*, **59**, 1067–1081.

Belousova, E., Griffin, W., O'Reilly, S.Y. and Fisher, N. (2002) Igneous zircon: trace element composition as

https://doi.org/10.1180/minmag.2017.081.012 Published online by Cambridge University Press

an indicator of source rock type. *Contributions to Mineralogy and Petrology*, **143**, 602–622.

Bindeman, I.N., Eiler, J.M., Yogodzinski, G.M., Tatsumi, Y., Stern, C.R., Grove, T.L., Portnyagin, M., Hoernle, K. and Danyushevsky, L.V. (2005) Oxygen isotope evidence for slab melting in modern and ancient subduction zones. *Earth and Planetary Science Letters*, **235**, 480–496.

Birch, W.D. (2008) Gem corundum from the St. Arnaud district, Western Victoria, Australia. *Australian Journal of Mineralogy*, **14**, 73–78.

Birch, W.D. and Henry, D.A. (1997) *Gem Minerals of Victoria, Melbourne*. Mineralogical Society of Victoria: Special Publication **No 4**, p. 40–41.

Birch, W.D., Fanning, M. and Magee, C. (2006) U-Pb dating of zircon and rutile from the gold-bearing White Hills Gravel, St Arnaud district, Victoria. *ASEG Extended Abstracts*, **2006**, 1–4.

Birch, W.D., Barron, L.M., Magee, C. and Sutherland, F. L. (2007) Gold- and diamond-bearing White Hills Gravel, St Arnaud district, Victoria: age and provenance based on U-Pb dating of zircon and rutile. *Australian Journal of Earth Sciences*, **54**, 609–628.

Black, L.P., Kamo, S.L., Allen, C.M., Davis, D.W., Aleinikoff, J.N., Valley, J.W., Mundil, R., Campbell, I. H., Korsch, R.J., Williams, I.S., *et al.* (2004) Improved 206Pb/238U microprobe geochronology by the monitoring of a trace-element-related matrix effect; SHRIMP, ID–TIMS, ELA–ICP–MS and oxygen isotope documentation for a series of zircon standards. *Chemical Geology*, **205**, 115–140.

Chualaowanich, T., Sutthirat, C., Pisutha-Arnond, V., Hauzenberger, C., Lo, C., Lee, T. and Charusiri, P. (2014) Geochemical characteristics and new eruption ages of ruby-related basalts from southeast Kenya. *Journal of Earth Science*, **25**, 799–821.

Claiborne, L.L., Miller, C.F., Walker, B.A., Wooden, J.L., Mazdab, F.K. and Bea, F. (2006) Tracking magmatic processes through Zr/Hf ratios in rocks and Hf and Ti zoning in zircons: An example from the Spirit Mountain batholith, Nevada. *Mineralogical Magazine*, **70**, 517–543.

Coenraads, R.R. (1994) Evaluation of potential sapphire source rocks within the catchments of Kings Plains Creek and Swan Brook, near Inverell, New South Wales. *Records of the Australian Museum*, **46**, 5–24.

Coenraads, R.R., Sutherland, F.L. and Kinny, P.D. (1990) The origin of sapphires: U-Pb dating of zircon inclusions sheds new light. *Mineralogical Magazine*, **54**, Part 1, 113–122.

Cohen, B.E. (2007) *High resolution 40Ar/39Ar geochronology of intraplate volcanism in Eastern Australia*. PhD Thesis, The University of Queensland.

Compston, W., Williams, I.S. and Meyer, C. (1984) U-Pb geochronology of zircons from lunar breccia 73217 using a sensitive high mass-resolution ion microprobe. *Journal of Geophysical Research: Solid Earth*, **89**, S02, B525–B534.

Criss, R.E. (1999) *Principles of Stable Isotope Distribution*. Oxford University Press.

Davies, D.R. and Rawlinson, N. (2014) On the origin of recent intraplate volcanism in Australia. *Geology*, **42**, 1031–1034.

Davies, D.R., Rawlinson, N., Iaffaldano, G. and Campbell, I.H. (2015) Lithospheric controls on magma composition along Earth/'s longest continental hotspot track. *Nature*, **525**, 511–514.

Dupuy, C., Liotard, J.M. and Dostal, J. (1992) Zr/Hf fractionation in intraplate basaltic rocks: Carbonate metasomatism in the mantle source. *Geochimica et Cosmochimica Acta*, **56**, 2417–2423.

Ewart, A., Chappell, B.W. and Menzies, M.A. (1988) An overview of the geochemical and isotopic characteristics of the Eastern Australian Cainozoic Volcanic provinces. *Journal of Petrology*, Special Volume, 225–273.

Fergusson, C.L. and Henderson, R.A. (2015) Early Palaeozoic continental growth in the Tasmanides of northeast Gondwana and its implications for Rodinia assembly and rifting. *Gondwana Research*, **28**(3) 933–953.

Fishwick, S., Heintz, M., Kennett, B.L.N. and Reading, A.M. (2008) Steps in lithospheric thickness within eastern Australia, evidence from surface wave tomography. *Tectonics*, **27**, TC4009.

Fritsch, E. and Rossman, G.R. (1987) An update on color in gems. Part 1: Introduction and colors caused by dispersed metal ions. *Gems & Gemology*, **23**, 126–139.

Fritsch, E. and Rossman, G.R. (1988) An update on color in gems. Part 2: Colors involving multiple atoms and color centers. *Gems & Gemology*, **24**, 3–14.

Fu, B., Page, F.Z., Cavosie, A.J., Fournelle, J., Kita, N.T., Lackey, J.S., Wilde, S.A. and Valley, J.W. (2008) Ti-in-zircon thermometry: applications and limitations. *Contributions to Mineralogy and Petrology*, **156**, 197–215.

Gaina, C., Müller, D.R., Royer, J.-Y. and Stock, J. (1998) The tectonic history of the Tasman Sea: A puzzle with 13 pieces. *Journal of Geophysical Research*, **103**, b6, 12413–12433.

Garnier, V., Ohnenstetter, D., Giuliani, G., Blanc, P. and Schwarz, D. (2002) Trace-element contents and cathodoluminescence of "trapiche" rubies from Mong Hsu, Myanmar (Burma): geological significance. *Mineralogy and Petrology*, **76**, 179–193.

Garnier, V., Ohnenstetter, D., Giuliani, G., Fallick, A.E., Trong, T.P., Quang, V.H., Van, L.P. and Schwarz, D. (2005) Basalt petrology, zircon ages and sapphire genesis from Dak Nong, southern Vietnam. *Mineralogical Magazine*, **69**, 21–38.

https://doi.org/10.1180/minmag.2017.081.012 Published online by Cambridge University Press

Giuliani, G., Fallick, A.E., Garnier, V., France-Lanord, C., Ohnenstetter, D. and Schwarz, D. (2005) Oxygen isotope composition as a tracer for the origins of rubies and sapphires. *Geology*, **33**, 249–252.

Giuliani, G., Fallick, A., Rakotondrazafy, M., Ohnenstetter, D., Andriamamonjy, A., Ralantoarison, T., Rakotosamizanany, S., Razanatseheno, M., Offant, Y., Garnier, V. *et al.* (2007) Oxygen isotope systematics of gem corundum deposits in Madagascar: relevance for their geological origin. *Mineralium Deposita*, **42**, 251–270.

Giuliani, G., Fallick, A.E., Ohnenstetter, D. and Pegere, G. (2009) Oxygen isotopes composition of sapphires from the French Massif Central: implications for the origin of gem corundum in basaltic fields. *Mineralium Deposita*, **44**, 221–231.

Giuliani, G., Ohnenstetter, D., Fallick, A.E., Groat, L.A. and Fagan, A.J. (2014) The geology and genesis of gem corundum deposits. Pp. 29–112 in: *Geology of Gem Deposits* (L.A. Groat, editor). Volume 44, Mineralogical Association of Canada (MAC), Canada.

Giuliani, G., Pivin, M., Fallick, A.E., Ohnenstetter, D., Song, Y. and Demaiffe, D. (2015) Geochemical and oxygen isotope signatures of mantle corundum megacrysts from the Mbuji-Mayi kimberlite, Democratic Republic of Congo, and the Changle alkali basalt, China. *Comptes Rendus Geoscience*, **347**, 24–34.

Glen, R.A. (2005) The Tasmanides of eastern Australia. Pp. 23–96 in: *Terrane Processes at the Margins of Gondwana* (A.P.M. Vaughan, P.T. Leat and R.J. Pankhurst, editors). Geological Society, London, Special Publications, **v. 246**.

Graham, I., Sutherland, L., Zaw, K., Nechaev, V. and Khanchuk, A. (2008) Advances in our understanding of the gem corundum deposits of the West Pacific continental margins intraplate basaltic fields. *Ore Geology Reviews*, **34**, 200–215.

Guo, J., O'Reilly, S.Y. and Griffin, W.L. (1996) Corundum from basaltic terrains: a mineral inclusion approach to the enigma. *Contributions to Mineralogy and Petrology*, **122**, 368–386.

Harlow, G. and Bender, W. (2013) A study of ruby (corundum) compositions from the Mogok Belt, Myanmar: Searching for chemical fingerprints. *American Mineralogist*, **98**, 1120–1132.

Henley, K. and Webb, A. (1990) *Radiometric dating on various granites and Newer Volcanics basalts.* Geological Survey of Victoria Unpublished Report, v. 27.

Hinton, R.W. and Upton, B.G.J. (1991) The chemistry of zircon: Variations within and between large crystals from syenite and alkali basalt xenoliths. *Geochimica et Cosmochimica Acta*, **55**, 3287–3302.

Hoskin, P.W.O. (2005) Trace-element composition of hydrothermal zircon and the alteration of Hadean zircon from the Jack Hills, Australia. *Geochimica et Cosmochimica Acta*, **69**, 637–648.

Izokh, A.E., Smirnov, S.Z., Egorova, V.V., Anh, T.T., Kovyazin, S.V., Phuong, N.T. and Kalinina, V.V. (2010) The conditions of formation of sapphire and zircon in the areas of alkali-basaltoid volcanism in Central Vietnam. *Russian Geology and Geophysics*, **51**, 719–733.

Johnson, R.W., Knutson, J. and Taylor, S.R. (1989) *Intraplate Volcanism in Eastern Australia and New Zealand*. Cambridge University Press, Cambridge, UK.

Khamloet, P., Pisutha-Arnond, V. and Sutthirat, C. (2014) Mineral inclusions in sapphire from the basalt-related deposit in Bo Phloi, Kanchanaburi, western Thailand: indication of their genesis. *Russian Geology and Geophysics*, **55**, 1087–1102.

Kogarko, L.N. (2016*a*) Fractionation of zirconium and hafnium during processes of mantle metasomatism. *Doklady Earth Sciences*, **468**, 598–601.

Kogarko, L.N. (2016*b*) Zirconium and hafnium fractionation in differentiation of alkali carbonatite magmatic systems. *Geology of Ore Deposits*, **58**, 173–181.

Levinson, A.A. and Cook, F.A. (1994) Gem corundum in Alkali basalt: origin and occurrence. *Gems and Gemology*, v. Winter, 253–262.

Limtrakun, P., Zaw, K., Ryan, C.G. and Mernagh, T.P. (2001) Formation of the Denchai gem sapphires, northern Thailand: evidence from mineral chemistry and fluid/melt inclusion characteristics. *Mineralogical Magazine*, **65**, 725–735.

Lishmund, S.R. and Oakes, G.M. (1989) Gemstones. Pp. 152–155 in: *Intraplate Volcanism in Eastern Australia and New Zealand* (R.W. Johnson, J. Knutson and S.R. Taylor, editors). Cambridge University Press, Cambridge.

Longerich, H.P., Jackson, S.E. and Gunther, D. (1996) Laser ablation inductively coupled plasma mass spectrometric transient signal data acquisition and analyte concentration calculation. *Journal of Analytical Atomic Spectrometry*, **11**, 899–904.

Ludwig, K.R. (2008) *User's Manual for ISOPLOT v3.70 A Geochronological Toolkit for Microsoft Excel*. Berkeley Geochronology Center, Special Publication **No. 4**, p. 76.

MacNevin, A.A. (1972) Sapphires in the New England district, New South Wales. *Records of the Geological Survey, NSW*, **14**, 19–35.

McGee, B.M. (2005) *Characteristics and Origin of the Weldborough Sapphire, NE Tasmania*. BSc Thesis, University of Tasmania, Australia.

Moon, A.R. and Phillips, M.R. (1984) An electron microscopy study of exsolved phases in natural black Australian sapphire. *Micron and Microscopica Acta*, **15**, 143–146.

https://doi.org/10.1180/minmag.2017.081.012 Published online by Cambridge University Press

Nassau, K. (2001) *The Physics and Chemistry of Color: The Fifteen Causes of Color*. Wiley, 504 p.

O'Reilly, S.Y. and Zhang, M. (1995) Geochemical characteristics of lava-field basalts from eastern Australia and inferred sources: connections with the subcontinental lithospheric mantle? *Contributions to Mineralogy and Petrology*, **121**, 148–170.

Palke, A.C., Renfro, N.D. and Berg, R.B. (2016) Origin of sapphires from a lamprophyre dike at Yogo Gulch, Montana, USA: Clues from their melt inclusions. *Lithos*, **260**, 339–344.

Paton, C., Hellstrom, J., Paul, B., Woodhead, J. and Hergt, J. (2011) Iolite: Freeware for the visualisation and processing of mass spectrometric data. *Journal of Analytical Atomic Spectrometry*, **26**, 2508–2518.

Pearce, N.J.G., Perkins, W.T., Westgate, J.A., Gorton, M. P., Jackson, S.E., Neal, C.R. and Chenery, S.P. (1997) A compilation of new and published major and trace element data for NIST SRM 610 and NIST SRM 612 glass reference materials. *Geostandards Newsletter*, **21**, 115–144.

Peucat, J.J., Ruffault, P., Fritsch, E., Bouhnik-Le Coz, M., Simonet, C. and Lasnier, B. (2007) Ga/Mg ratio as a new geochemical tool to differentiate magmatic from metamorphic blue sapphires. *Lithos*, **98**, 261–274.

Pham, V.L., Quang Vinh, H., Garnier, V., Giuliani, G., Ohnenstetter, D., Lhomme, T., Schwarz, D., Fallick, A., Dubessy, J. and Phan, T.T. (2004) Gem corundum deposits in Vietnam. *Journal of Gemmology*, **29**, 129–147.

Pisutha-Arnond, V., Hager, T., Atichat, W. and Wathanakul, P. (2006) The role of Be, Mg, Fe, and Ti in causing colour in corundum. *Journal of Gemmology*, **30**, 131–143.

Price, R.C., Nicholls, I.A. and Day, A. (2014) Lithospheric influences on magma compositions of late Mesozoic and Cenozoic intraplate basalts (the Older Volcanics) of Victoria, south-eastern Australia. *Lithos*, **206–207**, 179–200.

Rakotosamizanany, S., Giuliani, G., Ohnenstetter, D., Rakotondrazafy, A.F.M., Fallick, A.E., Paquette, J.-L. and Tiepolo, M. (2014) Chemical and oxygen isotopic compositions, age and origin of gem corundums in Madagascar alkali basalts. *Journal of African Earth Sciences*, **94**, 156–170.

Raymond, O.L., Liu, S., Gallagher, R., Zhang, W. and Highet, L.M. (2012) *Surface Geology of Australia 1:1 million scale dataset 2012 edition*. Commonwealth of Australia (Geoscience Australia), scale 1:1,000,000.

Robertson, A.D.C. and Sutherland, F.L. (1992) Possible origins and ages for sapphire and diamond from the Central Queensland gem fields. *Records of the Australian Museum*, **15**, 45–54.

Saminpanya, S. and Sutherland, F.L. (2011) Different origins of Thai area sapphire and ruby, derived from mineral inclusions and co-existing minerals. *European Journal of Mineralogy*, **23**, 683–694.

Saminpanya, S., Manning, D.A.C., Droop, G.T.R. and Henderson, C.M.B. (2003) Trace elements in Thai gem corundums. *Journal of Gemmology*, **28**, 392–398.

Schaltegger, U. (2007) Hydrothermal Zircon. *Elements*, **3**, 51–79.

Sharp, Z. (2007) *Principles of Stable Isotope Geochemistry.* Pearson Education, Upper Saddle River, NJ, USA.

Simonet, C., Paquette, J.L., Pin, C., Lasnier, B. and Fritsch, E. (2004) The Dusi (Garba Tula) sapphire deposit, Central Kenya – a unique Pan-African corundum-bearing monzonite. *Journal of African Earth Sciences*, **38**, 401–410.

Simonet, C., Fritsch, E. and Lasnier, B. (2008) A classification of gem corundum deposits aimed towards gem exploration. *Ore Geology Reviews*, **34**, 127–133.

Sláma, J., Košler, J., Condon, D.J., Crowley, J.L., Gerdes, A., Hanchar, J.M., Horstwood, M.S.A., Morris, G.A., Nasdala, L., Norberg, N. *et al.* (2008) Plešovice zircon – A new natural reference material for U–Pb and Hf isotopic microanalysis. *Chemical Geology*, **249**, 1–35.

Stähle, V., Frenzel, G., Kober, B., Michard, A., Puchelt, H. and Schneider, W. (1990) Zircon syenite pegmatites in the Finero peridotite (Ivrea zone): evidence for a syenite from a mantle source. *Earth and Planetary Science Letters*, **101**, 196–205.

Stephenson, P. (1976) Sapphire and zircon in some basaltic rocks from Queensland, Australia. Pp. 602–603 in: *Abstracts of the 25th International Geological Congress*, Sydney.

Stephenson, P., Burch-Johnston, A., Stanton, D. and Whitehead, P. (1998) Three long lava flows in north Queensland. *Journal of Geophysical Research: Solid Earth*, **103**, B11, 27359–27370.

Stern, R.J., Tsujimori, T., Harlow, G. and Groat, L.A. (2013) Plate tectonic gemstones. *Geology*, **41**, 723–726.

Sutherland, F.L. (1978) Mesozoic-Cainozoic volcanism of Australia. *Tectonophysics*, **48**, 413–427.

Sutherland, F.L. (1996) Alkaline rocks and gemstones, Australia: A review and synthesis. *Australian Journal of Earth Sciences*, **43**, 323–343.

Sutherland, F.L. and Abduriyim, A. (2009) Geographic typing of gem corundum; a test case from Australia. *Journal of Gemmology*, **31**, 203–210.

Sutherland, F.L. and Coenraads, R.R. (1996) An unusual ruby-sapphirine-spinel assemblage from the Tertiary Barrington volcanic province, New South Wales, Australia. *Mineralogical Magazine*, **60**, 623–638.

Sutherland, F.L. and Fanning, C.M. (2001) Gem-bearing basaltic volcanism, Barrington, New South Wales: Cenozoic evolution, based on basalt K–Ar ages and zircon fission track and U–Pb isotope dating. *Australian Journal of Earth Sciences*, **48**, 221–237.

Sutherland, F.L. and Wellman, P. (1986) Potassium-argon ages of tertiary volcanics rocks, Tasmania. *Papers and*

https://doi.org/10.1180/minmag.2017.081.012 Published online by Cambridge University Press

Proceedings of the Royal Society of Tasmania, **120**, 77–86.

Sutherland, F., Pogson, R., Hollis, J. and Flood, P. (1993) *Growth of the Central New England Basaltic Gemfields, New South Wales, based on Zircon Fission Track Dating*. Department of Geology and Geophysics, University of New England, Armidale, p. 483–491.

Sutherland, F.L., Hoskin, P.W.O., Fanning, C.M. and Coenraads, R.R. (1998*a*) Models of corundum origin from alkali basaltic terrains; a reappraisal. *Contributions to Mineralogy and Petrology*, **133**, 356–372.

Sutherland, F.L., Schwarz, D., Jobbins, E.A., Coenraads, R.R. and Webb, G. (1998*b*) Distinctive gem corundum suites from discrete basalt fields; a comparative study of Barrington, Australia, and West Pailin, Cambodia, gemfields. *Journal of Gemmology*, **26**, 65–85.

Sutherland, F.L., Graham, I.T., Pogson, R.E., Schwarz, D., Webb, G.B., Coenraads, R.R., Fanning, C.M., Hollis, J.D. and Allen, T.C. (2002) Tumbarumba basaltic gem field, New South Wales. In relation to sapphire-ruby deposits of Eastern Australia. *Records of the Australian Museum*, **54**, 215–248.

Sutherland, F.L., Coenraads, R.R., Schwarz, D., Raynor, L.R., Barron, B.J. and Webb, G.B. (2003) Al-rich diopside in alluvial ruby and corundum-bearing xenoliths, Australian and SE Asian basalt fields. *Mineralogical Magazine*, **67**, 717–732.

Sutherland, F.L., Duroc-Danner, J.M. and Meffre, S. (2008) Age and origin of gem corundum and zircon megacrysts from the Mercaderes-Rio Mayo area, south-west Colombia, South America. *Ore Geology Reviews*, **34**, 155–168.

Sutherland, F.L., Zaw, K., Meffre, S., Giuliani, G., Fallick, A.E., Graham, I.T. and Webb, G.B. (2009) Gem-corundum megacrysts from east Australian basalt fields: Trace elements, oxygen isotopes and origins. *Australian Journal of Earth Sciences*, **56**, 1003–1022.

Sutherland, F.L., Graham, I.T., Meffre, S., Zwingmann, H. and Pogson, R.E. (2012) Passive-margin prolonged volcanism, East Australian Plate: outbursts, progressions, plate controls and suggested causes. *Australian Journal of Earth Sciences*, **59**, 983–1005.

Sutherland, F.L., Graham, I.T., Hollis, J.D., Meffre, S., Zwingmann, H., Jourdan, F. and Pogson, R.E. (2014) Multiple felsic events within post-10 Ma volcanism, Southeast Australia: inputs in appraising proposed magmatic models. *Australian Journal of Earth Sciences*, **61**, 241–267.

Sutherland, F.L., Coenraads, R.R., Abduriyim, A., Meffre, S., Hoskin, P.W.O., Giuliani, G., Beattie, R., Wuhrer, R. and Sutherland, G.B. (2015) Corundum (sapphire) and zircon relationships, Lava Plains gem fields, NE Australia: integrated mineralogy, geochemistry, age determination, genesis and geographical typing. *Mineralogical Magazine*, **79**, 545–581.

Sutherland, L., Graham, I., Yaxley, G., Armstrong, R., Giuliani, G., Hoskin, P., Nechaev, V. and Woodhead, J. (2016) Major zircon megacryst suites of the Indo-Pacific lithospheric margin (ZIP) and their petrogenetic and regional implications. *Mineralogy and Petrology*, **109**, 1–22.

Upton, B.G.J. (1999) Megacrysts and associated Xenoliths: evidence for migration of geochemically enriched melts in the upper mantle beneath Scotland. *Journal of Petrology*, **40**, 935–955.

Vasconcelos, P.M., Knesel, K.M., Cohen, B.E. and Heim, J.A. (2008) Geochronology of the Australian Cenozoic: a history of tectonic and igneous activity, weathering, erosion, and sedimentation. *Australian Journal of Earth Sciences*, **55**, 865–914.

Vysotsky, S.V., Yakovenko, V.V., Ignat'ev, A.V. and Karabtsov, A.A. (2009) The oxygen isotopic composition as an indicator of the genesis of "Basaltic" corundum. *Russian Journal of Pacific Geology*, **3**, 64–68.

Watson, E.B., Wark, D.A. and Thomas, J.B. (2006) Crystallization thermometers for zircon and rutile. *Contributions to Mineralogy and Petrology*, **151**, 413–433.

Wellman, P. and McDougall, I. (1974) Cainozoic igneous activity in Eastern Australia. *Tectonophysics*, **23**, 49–65.

Wetherill, G.W. (1956) Discordant uranium-lead ages, I. *Eos, Transactions American Geophysical Union*, **37**, 320–326.

Yui, T.-F., Zaw, K. and Limtrakun, P. (2003) Oxygen isotope composition of the Denchai sapphire, Thailand: a clue to its enigmatic origin. *Lithos*, **67**, 153–161.

Yui, T.-F., Wu, C.-M., Limtrakun, P., Sricharn, W. and Boonsoong, A. (2006) Oxygen isotope studies on placer sapphire and ruby in the Chanthaburi-Trat alkali basaltic gemfield, Thailand. *Lithos*, **86**, 197–211.

Zaw, K., Sutherland, F.L., Dellapasqua, F., Ryan, C.G., Yui, T.-F., Mernagh, T.P. and Duncan, D. (2006) Contrasts in gem corundum characteristics, eastern Australian basaltic fields: trace elements, fluid/melt inclusions and oxygen isotopes. *Mineralogical Magazine*, **70**, 669–687.

Zaw, K., Sutherland, L., Yui, T.-F., Meffre, S. and Thu, K. (2015) Vanadium-rich ruby and sapphire within Mogok Gemfield, Myanmar: implications for gem color and genesis. *Mineralium Deposita*, **50**, 25–39.

Zhang, M., Stephenson, P.J., O'Reilly, S.Y., McCulloch, M.T. and Norman, M. (2001) Petrogenesis and Geodynamic implications of late Cenozoic basalts in North Queensland, Australia: Trace-element and Sr–Nd–Pb isotope evidence. *Journal of Petrology*, **42**, 685–719.

https://doi.org/10.1180/minmag.2017.081.012 Published online by Cambridge University Press